RESEARCH ARTICLE | DECEMBER 03 2018

Drag force and torque of a stationary sphere in a uniform laminar open channel flow

Lin Xie (谢琳) ; Qinghe Zhang (张庆河) ; Jinfeng Zhang (张金凤) ; Chunning Ji (及春宁)

Physics of Fluids 30, 123302 (2018)
https://doi.org/10.1063/1.5051789

Drag force and torque of a stationary sphere in a uniform laminar open channel flow

Lin Xie (谢琳), Qinghe Zhang (张庆河),[a] Jinfeng Zhang (张金凤), and Chunning Ji (及春宁)
State Key Laboratory of Hydraulic Engineering Simulation and Safety, Tianjin University, Tianjin 300072, China

(Received 13 August 2018; accepted 1 November 2018; published online 3 December 2018)

An analytical solution for a stationary sphere immersed in a steady and uniform laminar open channel flow with the surrounding fluid slowly passing by is presented. The solution satisfies the open channel boundary conditions by using a non-slip bottom wall and a free-slip top, and the non-slip condition on the sphere surface is achieved by a converged collocation method. The hydrodynamic drags and torques of the sphere located at different positions in the flow field are calculated. The results show that compared to Stokes' drag law, the drag force tends to be larger when the sphere is close to the bottom wall and smaller when closer to the slip top. The torque gradually changes from positive to negative as the distance from the bottom increases in an open channel flow. When the top boundary is set far enough from the sphere, the data results are consistent with those of a stationary sphere in a linear shear flow near a single wall. Approximate expressions for the drag force and torque with respect to the correlated length scales are fitted using the calculated results of the present solution, and the expressions can be simplified to single variable functions of the ratio between the sphere-bottom distance and the sphere radius h/a with sufficient accuracy when the water depth is considered to be infinite. *Published by AIP Publishing.* https://doi.org/10.1063/1.5051789

NOMENCLATURE

x, y, z	Streamwise, spanwise, and vertical Cartesian coordinates
r, θ, φ	Spherical coordinates
$\boldsymbol{r}$	Spherical coordinate vector
a	Radius of a sphere
H	Water depth
h	Interval between sphere center and bottom wall, also the height of the sphere center
ρ	Fluid density
μ	Dynamic viscosity
p	Pressure of the fluid
$\boldsymbol{T}$	Torque (vector)
$\boldsymbol{F}$	Hydrodynamic force (vector)
$\boldsymbol{u}$	Resultant fluid velocity vector
$\boldsymbol{u}_\infty, \boldsymbol{u}_s, \boldsymbol{u}_b$	Component velocity vector
$\boldsymbol{e}_x, \boldsymbol{e}_y, \boldsymbol{e}_z$	Unit vectors in x, y, z directions, respectively
u, v, w	Velocity components of $\mathbf{u}$ in x, y, z directions, respectively
$u_\infty, v_\infty, w_\infty$	Velocity components of $\boldsymbol{u}_\infty$ in x, y, z directions, respectively
u_s, v_s, w_s	Velocity components of $\boldsymbol{u}_s$ in x, y, z directions, respectively
u_b, v_b, w_b	Velocity components of $\boldsymbol{u}_b$ in x, y, z directions, respectively
$\chi_{-(n+1)}$	Solid spherical harmonics
$\phi_{-(n+1)}$	Solid spherical harmonics
$p_{-(n+1)}$	Solid spherical harmonics
$\mathrm{Re}_p, \mathrm{Re}_o$	Reynolds numbers
u_m	Maximum velocity of open channel flow
u_{sc}	Incoming velocity felt by a sphere
Π, Π_r	Stress tensors
P_n^m	Associated Legendre function
J_n	Bessel function of the first kind
K_ω	Modified Bessel function of the second kind
N	Number of points
n, m	Integers
σ	$=\kappa(z+h)$
τ	$=\kappa H$
α, β	Variables of Fourier integral
κ, γ	Integral variables
a_n, b_n, c_n	Constants
D_1, D_2, D_3	Functions of α, β, z
$\boldsymbol{M}$	Matrix of rank 3×6
$\boldsymbol{C}_{AB}$	Column matrix of 6 elements
$\boldsymbol{M}_i$	Row matrix of 6 elements ($i = 1, 2, 3$)
A_n^i, B_n^i, C_n^i	Functions of coordinates and n ($i = u, v, w$)
Λ_n^{ij}	Functions of coordinates and n ($i, j = 1, 2, 3$)
R_{in}, S_{in}, T_{in}	Functions ($i = 1, 2, 3, 4, 5, 6$)
A_i, B_i	Functions of α, β, z ($i = a, b, c$)
$A_n'^j, B_n'^j, C_n'^j$	Functions of coordinates and n ($j = u, v, w$)
F_{Stokes}	Stokes drag
F_1–F_4	Functions of κ, γ
ζ_n^{ij}	Functions of κ, x, y, z ($i, j = 1, 2, 3$)
F_x	Force in the x direction
T_y	Torque in the y direction
f_x^{s*}, f_x^*	Nondimensional force
t_y^{s*}, t_y^*	Nondimensional torque
q_n, Q_n	Expressions independent of h and H

I. INTRODUCTION

The topic of sediment transport caused by water flow has attracted considerable attention in the field of river and ocean

[a]Author to whom correspondence should be addressed: qhzhang@tju.edu.cn

dynamics. Several studies associated with theoretical analyses (Dey, 2014), experiments (Ikeda and Mcewan, 2009), numerical simulations (Merritt *et al.*, 2003), and *in situ* measurements (Villar *et al.*, 2012) have been conducted by researchers to study sediment transport. During the past two decades, Particle Resolved Simulations (PRSs) and the Lagrangian model of the point sphere method, the Discrete Particle Model (DPM), have become widely used (Esteghamatian *et al.*, 2017) for the fluid-particle system. In view of the unbearable computation load of PRSs, DPM is popular in sediment transport research (Drake and Calantoni, 2001; Henry and Minier, 2014; Sun and Xiao, 2016; and Liu *et al.*, 2017). For the fluid-particle system, hydrodynamic interaction is essential and attractive (Daddi-Moussa-Ider *et al.*, 2017; Felderhof, 2017; and Turkyilmazoglu, 2018). Applying accurate hydrodynamic forces, especially the drag force on a sediment particle, is a key issue in the DPM. At present, many force expressions have been used in the DPM. Liu *et al.* (2017) chose an approximate expression of the relationship of the drag and the Reynolds number for an unbounded sphere proposed by Morsi and Alexander (1972) to calculate the sediment entrainment in a turbulent open channel flow. Xu *et al.* (2000) and Guo *et al.* (2013) adopted Di Felice's drag model (DiFelice, 1994), which is based on experimental data for a hindered sphere with different Reynolds numbers, used for a fluidized bed simulation. Kloss *et al.* (2012) applied another empirical force formula proposed by Gidaspow *et al.* (1986), who combined two equations from Ergun (1952) and Wen and Yu (1966). Sun and Xiao (2016) conducted a simulation on sediment transportation in an oscillatory sheet flow based on Syamlal's empirical model (Nielsen, 1992) for a system of multiple-particle phases. Alobaid *et al.* (2013) estimated the hydrodynamic behavior of a gas-solid flow in a 3D circulating fluidized bed using the hindered drag-Reynolds number relationship obtained from the numerical results of Hill *et al.* (2001). Beetstra *et al.* (2007a) applied their own drag model (Beetstra *et al.*, 2007b) to a polydisperse system to perform discrete particle simulations of a segregating system. Renzo *et al.* (2011) adopted another drag model for a polydisperse system from the numerical data by Cello *et al.* (2010). Although many drag models have been proposed and applied to the above DPMs, none of them considered the wall effect, which plays an important role in the extremely important near-bed region (Henry and Minier, 2014).

In practice, the wall effect on the hydrodynamic forces of particles near the bed is apparent (Chan-Braun *et al.*, 2011). Two hydrodynamic mechanisms are induced near the wall according to Takemura and Magnaudet (2003) and Zeng *et al.* (2005): one is the break of symmetry in the flow distribution, and the other is an acceleration of the fluid in the gap between the sphere and the wall. The drag of a sphere touching a wall in a linear shear flow (Lee and Balachandar, 2017; O'Neill, 1968; and Zeng *et al.*, 2009) can increase by approximately 70% compared to that of a sphere in an unbounded linear shear flow (Dandy and Dwyer, 1990) across a Reynolds number range of (0, 100). In a creeping flow condition, O'Neill (1968) derived the drag expression of a sphere fixed on a wall in a linear shear flow, and Goldman *et al.* (1967) provided a table of the exact drag force for varying separation distances between the sphere and the wall under a linear shear flow. For a finite Reynolds number, Zeng *et al.* (2009) simulated the hydrodynamic forces of a sphere proximate to a wall in a linear shear flow and proposed a Reynolds number correction based on expressions by Goldman *et al.* (1967) and Lee and Balachandar (2017) conducted simulations of the rough-wall bounded condition, showing that the results of the force expressions of Zeng *et al.* (2009) for a smooth-wall condition are still appropriate for a rough-wall condition.

Most of the above modifications of the drag force formulae for near-bed particles are for stationary particles in a linear shear flow or moving particles in a quiescent flow. At present, drag force formulae for near-bed particles in an open channel flow are scarce, though a few investigations on the relationship between the hydrodynamic force on a sphere and its surrounding flow field have been conducted. Dwivedi *et al.* (2010) conducted experiments relating the drag force of a sediment particle to the point velocity. Amir *et al.* (2014) measured the pressure forces on sediment particles on the bed of an open channel flow for different flow depths and bed slopes. Using the particle-resolved numerical simulation method, Chan-Braun *et al.* (2013; 2011) investigated the force and torque acting on fixed particles that formed the rough bed of an open channel flow and analyzed the correlation between the particle drag and the pressure field and the near wall turbulence. Ji *et al.* (2013) showed the statistical features of hydrodynamic forces of sediment particles in a turbulent open channel flow in the bed-load regime. The above studies revealed the dependency characteristics between the hydrodynamic force and the near wall flow field; however, they are incapable of providing the applicable force formula for near-bed particles in an open channel flow. Hence, this paper aims to derive the force and torque expressions for a sphere near the bed in an open channel flow with a low Reynolds number and to provide a force model for a near-bed sediment transport using DPMs. The remainder of the paper is structured as follows. In Sec. II, the mathematical formulations, including governing equations, general solutions, and the solution process for a sphere in an open channel flow with a low Reynolds number, are presented. The calculated values of the drag force and torque under different depths of water and sphere locations are provided in Sec. III, as well as discussions of the effect of boundaries on forces. The approximate expressions for the drag and torque are given in Sec. IV, and conclusions are drawn in Sec. V.

II. MATHEMATICAL FORMULATION

In this paper, a steady and uniform open channel flow of the velocity field $\boldsymbol{u}_\infty$, density ρ, and kinematic viscosity ν under a laminar flow condition is considered. The free surface boundary is simplified to a free-slip plane parallel to the bottom wall. A sphere of radius a with an interval h between the sphere center and the bottom wall is immersed in the open channel flow with water depth H. The general setup of the problem is displayed in Fig. 1. For convenience of derivation, two sets of coordinate systems, Cartesian coordinates (x, y, z) and spherical coordinates (r, θ, φ), are used. The origins of the two coordinates coincide at the sphere center. Then, the problem of a steady and uniform open channel flow $\boldsymbol{u}_\infty$ under

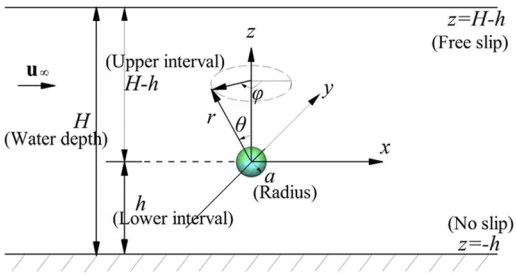

FIG. 1. Geometric sketch of a sphere with radius a suspended a certain distance h from the bottom wall in an open channel flow. The bottom wall is planar, and a parallel plane with a free-slip boundary condition is set at H to form an open channel.

a laminar flow condition slowly passing the sphere is to be solved. In this paper, a sphere of radius a is chosen as the characteristic length used to nondimensionalize the other length variables; the most frequently used length variables are one height and two main intervals nondimensionalized by radius a: the nondimensional height of the water depth is H/a, the nondimensional lower interval is h/a, and the nondimensional upper interval is $(H-h)/a$, where h is the interval between the sphere center and the bottom wall of the open channel and $(H-h)$ is the interval between the sphere center and the top surface of the open channel.

A. Governing equations and boundary conditions

In the present research, a steady-uniform-laminar open channel flow $\boldsymbol{u}_\infty$, whose local and convective acceleration is both zero, slowly passes by a sphere and forms the target flow $\boldsymbol{u}$. When the flow around the sphere and near the bottom wall can be regarded as a creeping flow and the remaining flow is a steady-uniform-laminar open channel flow, then the target fluid motion is governed by the linearized N-S equations,

$$\nu\,\nabla^2\boldsymbol{u} = \frac{1}{\rho}\nabla p, \tag{1a}$$

$$\nabla\cdot\boldsymbol{u} = 0, \tag{1b}$$

where $\boldsymbol{u} = u\boldsymbol{e}_x + v\boldsymbol{e}_y + w\boldsymbol{e}_z$ is the velocity field, in which $\boldsymbol{e}_x$, $\boldsymbol{e}_y$, and $\boldsymbol{e}_z$ are the unit vectors of Cartesian coordinates in the x, y, and z directions, respectively; and p is the pressure. The boundary conditions for the fluid velocity at the bottom wall, upper boundary plane, sphere surface, and infinite bounding are, respectively,

$$z=-h: \quad u=v=w=0, \tag{2a}$$

$$z=H-h: \quad w=0, \quad \frac{\partial u}{\partial z}=0, \quad \frac{\partial v}{\partial z}=0, \tag{2b}$$

$$r=a: \quad u=v=w=0, \tag{2c}$$

$$\sqrt{x^2+y^2}\to\infty: \quad \frac{\partial \boldsymbol{u}}{\partial x}=0, \quad \frac{\partial \boldsymbol{u}}{\partial y}=0. \tag{2d}$$

When the undisturbed upstream velocity at the height of the sphere center u_{sc} is used to define the Reynolds number $\mathrm{Re}_p = \frac{2u_{sc}a}{\nu}$, which is often named the particle Reynolds number. $\mathrm{Re}_p \ll 1$ represents a slowly incoming velocity to the sphere and the near bed region, and necessarily denotes a creeping flow condition near the sphere and the near bed region. That is to say, the present research is limited to steady-uniform-laminar open channel flow and a low particle Reynolds number of $\mathrm{Re}_p \ll 1$.

B. General solutions of the velocity

The velocity field $\boldsymbol{u}$ can be expressed as a linear superposition of three contributions (Ganatos *et al.*, 1980), where each part independently satisfies Eq. (1),

$$\boldsymbol{u} = \boldsymbol{u}_\infty + \boldsymbol{u}_s + \boldsymbol{u}_b, \tag{3}$$

where $\boldsymbol{u}_\infty$ represents the unidirectional velocity without the sphere under an external pressure drive. This velocity independently satisfies the momentum (1a) and continuity (1b) equations. By applying the upper (2b), the bottom (2a), and the streamwise and spanwise (2d) boundary conditions, $\boldsymbol{u}_\infty$ is uniquely determined using Eq. (4b) for a steady and uniform laminar open channel flow

$$\boldsymbol{u}_\infty = u_\infty\boldsymbol{e}_x + v_\infty\boldsymbol{e}_y + w_\infty\boldsymbol{e}_z, \tag{4a}$$

$$u_\infty = u_m\left[2\frac{z+h}{H} - \left(\frac{z+h}{H}\right)^2\right], \quad v_\infty = w_\infty = 0, \tag{4b}$$

where u_∞, v_∞, and w_∞ represent the three components of $\boldsymbol{u}_\infty$ and u_m represents the maximum velocity, which is chosen as the characteristic velocity.

The second part of $\boldsymbol{u}$ in Eq. (3), denoted by $\boldsymbol{u}_s$, is a general solution of Eq. (1) in spherical coordinates with planar symmetry about the plane $y=0$ and satisfies $\boldsymbol{u}_s = 0$ at $r\to\infty$. It is written as an infinite series as described by Eq. (6). The maximum velocity of $\boldsymbol{u}_s$ is comparable to u_{sc} and the disturbance field $\boldsymbol{u}_s$ could be regarded as creeping motion when u_{sc} is small

$$\boldsymbol{u}_s = u_s\boldsymbol{e}_x + v_s\boldsymbol{e}_y + w_s\boldsymbol{e}_z, \tag{5}$$

where

$$u_s = \sum_{n=1}^{\infty}\left(a_nA_n^u + b_nB_n^u + c_nC_n^u\right), \tag{6a}$$

$$v_s = \sum_{n=1}^{\infty}\left(a_nA_n^v + b_nB_n^v + c_nC_n^v\right), \tag{6b}$$

$$w_s = \sum_{n=1}^{\infty}\left(a_nA_n^w + b_nB_n^w + c_nC_n^w\right), \tag{6c}$$

where A_n^i, B_n^i, and C_n^i $(i = u, v, w)$ are functions of the position involving the associated Legendre functions listed in Appendix A, which were also given by Eq. (2.6) in Ganatos *et al.* (1980). a_n, b_n, and c_n are unknown constants to be determined by the boundary conditions. Expressions of A_n^i, B_n^i, and C_n^i could be derived from the fundamental solution of Eqs. (1a) and (1b) for the situation where the flow is exterior to a sphere. The fundamental solution given by Happel and Brenner (1983) is expressed as

$$\boldsymbol{u}_s = \sum_{n=1}^{\infty}\left[\nabla\times(\boldsymbol{r}\chi_{-(n+1)}) + \nabla\phi_{-(n+1)} - \frac{n-2}{\mu 2n(2n-1)}r^2\nabla p_{-(n+1)} + \frac{n+1}{\mu n(2n-1)}\boldsymbol{r}p_{-(n+1)}\right], \tag{7a}$$

$$p_s = \sum_{n=1}^{\infty}p_{-(n+1)}, \tag{7b}$$

where $\chi_{-(n+1)}$, $\phi_{-(n+1)}$, and $p_{-(n+1)}$ are solid spherical harmonics of order $-(n+1)$, $\boldsymbol{r}$ is the spherical coordinate vector with its origin at the center of the sphere, and p_s is the pressure of the disturbance. According to Ganatos *et al.* (1980), when the flow is symmetric about the plane $y = 0$ with a stationary sphere, the three functions in Ganatos (1978) are formulated as

$$\chi_{-(n+1)} = \mathrm{P}_n^1(\cos\theta)\frac{1}{r^{n+1}}c_n \sin\phi, \tag{8a}$$

$$\phi_{-(n+1)} = \mathrm{P}_n^1(\cos\theta)\frac{1}{r^{n+1}}b_n \cos\phi, \tag{8b}$$

$$p_{-(n+1)} = \mathrm{P}_n^1(\cos\theta)\frac{1}{r^{n+1}}\mu a_n \cos\phi, \tag{8c}$$

where r, θ, and φ are the spherical coordinates and P_n^m is the associated Legendre function of order n and degree m. Substituting Eq. (8) into Eq. (7) and rearranging $\boldsymbol{u}_s$ to match the forms in Eq. (6), we obtain detailed expressions of A_n^i, B_n^i, and C_n^i ($i = u, v, w$) (see Appendix A).

The third part of $\boldsymbol{u}$ in Eq. (3), denoted by $\boldsymbol{u}_b$, is also a general solution of Eq. (1). It is given in the double Fourier integral forms in Cartesian coordinates by Eqs. (10) and (11). It produces finite velocities everywhere in the flow field controlled by Eq. (1). With a proper choice of its undetermined functions in $\boldsymbol{C}_{AB}$ in Eq. (11a), $\boldsymbol{u}_b$ could exactly balance the disturbance caused by $\boldsymbol{u}_s$ along the upper and bottom boundaries to make the resultant velocity ($\boldsymbol{u}_b$+$\boldsymbol{u}_s$) exactly satisfy the target boundary conditions

$$\boldsymbol{u}_b = u_b\boldsymbol{e}_x + v_b\boldsymbol{e}_y + w_b\boldsymbol{e}_z, \tag{9}$$

where u_b, v_b, and w_b are given by the double Fourier integrals (Ganatos *et al.*, 1980)

$$u_b = \int_0^\infty\int_0^\infty D_1(\alpha,\beta,z)\cos\alpha x\cos\beta y\mathrm{d}\alpha\mathrm{d}\beta, \tag{10a}$$

$$v_b = \int_0^\infty\int_0^\infty D_2(\alpha,\beta,z)\sin\alpha x\sin\beta y\mathrm{d}\alpha\mathrm{d}\beta, \tag{10b}$$

$$w_b = \int_0^\infty\int_0^\infty D_3(\alpha,\beta,z)\sin\alpha x\cos\beta y\mathrm{d}\alpha\mathrm{d}\beta, \tag{10c}$$

where

$$\begin{pmatrix} D_1(\alpha,\beta,z)\\ D_2(\alpha,\beta,z)\\ D_3(\alpha,\beta,z)\end{pmatrix} = \begin{pmatrix} \boldsymbol{M}_1(\alpha,\beta,z)\\ \boldsymbol{M}_2(\alpha,\beta,z)\\ \boldsymbol{M}_3(\alpha,\beta,z)\end{pmatrix}\cdot\boldsymbol{C}_{AB}, \tag{11a}$$

$$\begin{pmatrix} \boldsymbol{M}_1(\alpha,\beta,z)\\ \boldsymbol{M}_2(\alpha,\beta,z)\\ \boldsymbol{M}_3(\alpha,\beta,z)\end{pmatrix} = \begin{pmatrix} \frac{\mathrm{e}^{z\kappa}}{\kappa}\left(\kappa+z\alpha^2\right) & -\frac{\mathrm{e}^{z\kappa}z\alpha\beta}{\kappa} & -\mathrm{e}^{z\kappa}z\alpha & \frac{\mathrm{e}^{-z\kappa}}{\kappa}\left(\kappa-z\alpha^2\right) & \frac{\mathrm{e}^{-z\kappa}z\alpha\beta}{\kappa} & -\mathrm{e}^{-z\kappa}z\alpha\\ -\frac{\mathrm{e}^{z\kappa}z\alpha\beta}{\kappa} & \frac{\mathrm{e}^{z\kappa}}{\kappa}\left(\kappa+z\beta^2\right) & \mathrm{e}^{z\kappa}z\beta & \frac{\mathrm{e}^{-z\kappa}z\alpha\beta}{\kappa} & \frac{\mathrm{e}^{-z\kappa}}{\kappa}\left(\kappa-z\beta^2\right) & \mathrm{e}^{-z\kappa}z\beta\\ \mathrm{e}^{z\kappa}z\alpha & -\mathrm{e}^{z\kappa}z\beta & \mathrm{e}^{z\kappa}(1-z\kappa) & \mathrm{e}^{-z\kappa}z\alpha & -\mathrm{e}^{-z\kappa}z\beta & \mathrm{e}^{-z\kappa}(1+z\kappa)\end{pmatrix}, \tag{11b}$$

and where $\boldsymbol{C}_{AB}$, denoting a column matrix $(A_a, A_b, A_c, B_a, B_b, B_c)^{\mathrm{T}}$, is a column of unknown functions of separation variables α and β, $\kappa = \sqrt{\alpha^2+\beta^2}$ in Eq. (11b).

C. Force and torque on the sphere

Here, we define the disturbance field $\boldsymbol{u}_s$ generated by the sphere as the reacting field, and $\boldsymbol{u}_b$ and $\boldsymbol{u}_\infty$ as the external acting fields. Then, with the knowledge of the reacting field $\boldsymbol{u}_s$, the reacting stress tensor along the radial direction can be expressed as

$$\Pi_r = \frac{\boldsymbol{r}}{r}\cdot\Pi = -\frac{\boldsymbol{r}}{r}p_s + \frac{\mu}{r}\boldsymbol{r}\cdot\left(\nabla\boldsymbol{u}_s + \nabla\boldsymbol{u}_s{}^{\mathrm{T}}\right), \tag{12}$$

where $\boldsymbol{r}$ is a vector in the radial direction.

When $\boldsymbol{u}_s$ satisfies Eq. (7), Π_r can be simplified according to the relation $\boldsymbol{r}\cdot\left(\nabla\boldsymbol{u}_s + \nabla\boldsymbol{u}_s{}^{\mathrm{T}}\right) = \nabla(\boldsymbol{r}\cdot\boldsymbol{u}_s) - \boldsymbol{u}_s + (\boldsymbol{r}\cdot\nabla)\boldsymbol{u}_s$,

$$\Pi_r = \frac{\mu}{r}\sum_{n=1}^{\infty}\Bigg[-(n+2)\nabla\times(\boldsymbol{r}\chi_{-(n+1)}) - (2n+3)\nabla\phi_{-(n+1)} - \frac{1}{\mu}\frac{2n^2+1}{n(2n-1)}\boldsymbol{r}p_{-(n+1)} + \frac{r^2}{2\mu}\nabla p_{-(n+1)}\Bigg], \tag{13a}$$

$$\boldsymbol{r}\times\Pi_r = \frac{\mu}{r}\sum_{n=1}^{\infty} \times\begin{bmatrix} -(n+2)\left(r^2\nabla\chi_{-(n+1)}\right) - (n+2)(n+1)\boldsymbol{r}\chi_{-(n+1)}\\ +(2n+3)\nabla\times(\boldsymbol{r}\phi_{-(n+1)}) - \frac{r^2}{2\mu}\nabla\times(\boldsymbol{r}p_{-(n+1)})\end{bmatrix}. \tag{13b}$$

Since $\boldsymbol{u}_b$ and $\boldsymbol{u}_\infty$ are external acting fields without the immersion of the sphere, there are no direct hydrodynamic forces between the two fields and the sphere. Therefore, $\boldsymbol{u}_b$ and $\boldsymbol{u}_\infty$ do not change the expressions of the force and torque on the sphere but indirectly affect the magnitude of the expressions by influencing the value of $\boldsymbol{u}_s$ as an external action. Then, according to Happel and Brenner (1983), the expressions of the reacting drag force and torque generated by the sphere can be obtained by integrating the above stress in Eq. (13) around the sphere surface as $\boldsymbol{F} = \int_S \Pi_r \mathrm{d}S$, $\boldsymbol{T} = \int_S \boldsymbol{r}\times\Pi_r \mathrm{d}S$ [where S denotes the sphere surface and $\mathrm{d}S$ ($=r^2\sin\theta\,\mathrm{d}\theta\,\mathrm{d}\varphi$) denotes an element of a surface area on a sphere]. According to the surface integral theorems listed in Happel and Brenner (1983),

$$\int_S \lambda_n \mathrm{d}S = \begin{cases} 4\pi r^2 \lambda_0, & n = 0 \\ 4\pi r^2 \lambda_{-1}, & n = -1 \\ 0, & \text{else} \end{cases}, \tag{14a}$$

$$\int_S \boldsymbol{r}\lambda_n \mathrm{d}S = \begin{cases} \dfrac{4\pi r^4}{3}\nabla\lambda_1, & n = 1 \\ \dfrac{4\pi r}{3}\nabla\left(r^3\lambda_{-2}\right), & n = -2 \\ 0, & \text{else} \end{cases}, \tag{14b}$$

$$\int_S \nabla\lambda_n \mathrm{d}S = \begin{cases} 4\pi r^2 \nabla\lambda_1, & n = 1 \\ 0, & \text{else} \end{cases}, \tag{14c}$$

$$\int_S \nabla \times (\boldsymbol{r}\lambda_n)\mathrm{d}S = 0, \tag{14d}$$

where λ_n is any solid spherical function of order n. The reacting hydrodynamic force and torque can be easily obtained as $\boldsymbol{F} = -4\pi\nabla\left(r^3 p_{-2}\right)$ and $\boldsymbol{T} = -8\pi\mu\nabla\left(r^3\chi_{-2}\right)$, respectively. Then, the acting drag force (drag exerted on the sphere by the external flow field) and acting torque (torque exerted on the sphere by the external flow field) are easy to obtain using Newton's third law. In this paper, we focus on the acting drag along the x direction F_x ($=-\boldsymbol{F}\cdot\boldsymbol{e}_x$) and the acting torque along the y direction T_y ($=-\boldsymbol{T}\cdot\boldsymbol{e}_y$). When substituting the expressions of p_{-2} (8c) and χ_{-2} (8a), F_x and T_y could be further written as

$$F_x = 4\pi\mu a_1, \tag{15a}$$

$$T_y = 8\pi\mu c_1 \boldsymbol{e}_y, \tag{15b}$$

where constants a_1 and c_1, namely, the first order of a_n, b_n, and c_n in Eq. (6), are determined by satisfying the boundary conditions in Eq. (2).

D. Determination of the unknown functions C_{AB} and constants (a_n, b_n, c_n)

To obtain the ultimate solution of $\boldsymbol{u}$, we need to solve two groups of unknown quantities, namely, one group of unknown functions $\boldsymbol{C}_{AB}$ in $\boldsymbol{u}_b$ and another group of unknown constants (a_n, b_n, c_n) in $\boldsymbol{u}_s$. We can obtain $\boldsymbol{C}_{AB}$ by applying the upper and the bottom boundary conditions, and we obtain a_n, b_n, and c_n by applying the sphere surface boundary condition. The upper and bottom boundary conditions are satisfied analytically with the detailed derivations below, and the sphere surface boundary conditions are applied according to the collocation technique in Ganatos *et al.* (1980); this technique is complemented by applying the sphere surface boundary conditions at N points on the sphere's surface and generating a group of $3N$ linear algebraic equations.

1. Determination of unknown functions C_{AB} for u_b

According to the upper and bottom boundary conditions in Eqs. (2a) and (2b), velocities u ($=u_\infty + u_b + u_s$), v ($=v_\infty + v_b + v_s$), and w ($=w_\infty + w_b + w_s$) satisfy

$$u = 0,\ v = 0,\ w = 0,\ \text{at } z = -h, \tag{16a}$$

$$\frac{\partial u}{\partial z} = 0,\ \frac{\partial v}{\partial z} = 0,\ w = 0,\ \text{at } z = H - h, \tag{16b}$$

while $\boldsymbol{u}_\infty$ also independently satisfies these boundary conditions,

$$u_\infty = v_\infty = w_\infty = 0,\ \text{at } z = -h, \tag{17a}$$

$$\frac{\partial u_\infty}{\partial z} = 0,\ \frac{\partial v_\infty}{\partial z} = 0,\ w_\infty = 0,\ \text{at } z = H - h, \tag{17b}$$

we then have

$$u_b + u_s = 0,\ v_b + v_s = 0,\ w_b + w_s = 0,\ \text{at } z = -h, \tag{18a}$$

$$\frac{\partial u_b}{\partial z} + \frac{\partial u_s}{\partial z} = 0,\ \frac{\partial v_b}{\partial z} + \frac{\partial v_s}{\partial z} = 0,\ w_b + w_s = 0,\ \text{at } z = H - h. \tag{18b}$$

Substituting the expressions of u_s, v_s, and w_s in Eq. (6) and u_b, v_b, and w_b in Eqs. (10) and (11) into the above expressions, we obtain the following 6 equations:

$$\int_0^\infty\int_0^\infty \frac{\partial}{\partial z}D_1(\alpha,\beta,z)\Big|_{z=H-h}\cos\alpha x\cos\beta y\mathrm{d}\alpha\mathrm{d}\beta + \sum_{n=1}^{\infty}\left[a_n\frac{\partial}{\partial z}A_n^u(x,y,z) + b_n\frac{\partial}{\partial z}B_n^u(x,y,z) + c_n\frac{\partial}{\partial z}C_n^u(x,y,z)\right]\Big|_{z=H-h} = 0, \tag{19a}$$

$$\int_0^\infty\int_0^\infty \frac{\partial}{\partial z}D_2(\alpha,\beta,z)\Big|_{z=H-h}\sin\alpha x\sin\beta y\mathrm{d}\alpha\mathrm{d}\beta + \sum_{n=1}^{\infty}\left[a_n\frac{\partial}{\partial z}A_n^v(x,y,z) + b_n\frac{\partial}{\partial z}B_n^v(x,y,z) + c_n\frac{\partial}{\partial z}C_n^v(x,y,z)\right]\Big|_{z=H-h} = 0, \tag{19b}$$

$$\int_0^\infty\int_0^\infty D_3(\alpha,\beta,H-h)\sin\alpha x\cos\beta y\mathrm{d}\alpha\mathrm{d}\beta + \sum_{n=1}^{\infty}\left[a_nA_n^w(x,y,z) + b_nB_n^w(x,y,z) + c_nC_n^w(x,y,z)\right]\Big|_{z=H-h} = 0, \tag{19c}$$

$$\int_0^\infty\int_0^\infty D_1(\alpha,\beta,-h)\cos\alpha x\cos\beta y\mathrm{d}\alpha\mathrm{d}\beta + \sum_{n=1}^{\infty}\left[a_nA_n^u(x,y,z) + b_nB_n^u(x,y,z) + c_nC_n^u(x,y,z)\right]\Big|_{z=-h} = 0, \tag{19d}$$

$$\int_0^\infty\int_0^\infty D_2(\alpha,\beta,-h)\sin\alpha x\sin\beta y\mathrm{d}\alpha\mathrm{d}\beta + \sum_{n=1}^{\infty}\left[a_nA_n^v(x,y,z) + b_nB_n^v(x,y,z) + c_nC_n^v(x,y,z)\right]\Big|_{z=-h} = 0, \tag{19e}$$

$$\int_0^\infty\int_0^\infty D_3(\alpha,\beta,-h)\sin\alpha x\cos\beta y\mathrm{d}\alpha\mathrm{d}\beta + \sum_{n=1}^{\infty}\left[a_nA_n^w(x,y,z) + b_nB_n^w(x,y,z) + c_nC_n^w(x,y,z)\right]\Big|_{z=-h} = 0, \tag{19f}$$

and

$$\begin{pmatrix} \frac{\partial}{\partial z}D_1(\alpha,\beta,z)\Big|_{z=H-h} \\ \frac{\partial}{\partial z}D_2(\alpha,\beta,z)\Big|_{z=H-h} \\ D_3(\alpha,\beta,H-h) \\ D_1(\alpha,\beta,-h) \\ D_2(\alpha,\beta,-h) \\ D_3(\alpha,\beta,-h) \end{pmatrix} = \begin{pmatrix} \frac{\partial}{\partial z}\boldsymbol{M}_1(\alpha,\beta,z)\Big|_{z=H-h} \\ \frac{\partial}{\partial z}\boldsymbol{M}_2(\alpha,\beta,z)\Big|_{z=H-h} \\ \boldsymbol{M}_3(\alpha,\beta,H-h) \\ \boldsymbol{M}_1(\alpha,\beta,-h) \\ \boldsymbol{M}_2(\alpha,\beta,-h) \\ \boldsymbol{M}_3(\alpha,\beta,-h) \end{pmatrix} \cdot \boldsymbol{C}_{AB}. \tag{20}$$

In Eqs. (19) and (20), the elements of $\boldsymbol{C}_{AB}$ need to be solved. Since the matrix $\boldsymbol{M}$ is known in Eq. (11b), after solving the intermediate functions $\frac{\partial}{\partial z}D_1(\alpha,\beta,z)\big|_{z=H-h}$, $\frac{\partial}{\partial z}D_2(\alpha,\beta,z)\big|_{z=H-h}$, $D_3(\alpha,\beta,H-h)$, $D_1(\alpha,\beta,-h)$, $D_2(\alpha,\beta,-h)$, and $D_3(\alpha,\beta,-h)$ using Eq. (19), $\boldsymbol{C}_{AB}$ is within reach based on Eq. (20).

According to the definitions of the Fourier cosine (sine) transform, $F(\omega)=\int_0^\infty f(t)\sin\omega t\mathrm{d}t$ ($F(\omega)=\int_0^\infty f(t)\cos\omega t\mathrm{d}t$) is the cosine (sine) transform of $f(t)$, and $f(t)=\frac{2}{\pi}\int_0^\infty F(\omega)\sin\omega t\mathrm{d}\omega$ ($f(t)=\frac{2}{\pi}\int_0^\infty F(\omega)\sin\omega t\mathrm{d}\omega$) is the inverse cosine (sine) transform of $F(\omega)$. The 6 intermediate functions $\frac{\partial D_1(\alpha,\beta,z)}{\partial z}\Big|_{z=H-h}$, $\frac{\partial D_2(\alpha,\beta,z)}{\partial z}\Big|_{z=H-h}$, $D_3(\alpha,\beta,H-h)$, $D_1(\alpha,\beta,-h)$, $D_2(\alpha,\beta,-h)$, and $D_3(\alpha,\beta,-h)$ can be expressed in terms of the coefficients a_n, b_n, and c_n via double inverse transformations of the disturbances produced by the sphere. Using the functions R_{in}, S_{in}, and T_{in} ($i=1,2,3,4,5,6$) listed in Appendix B to replace the long expressions of the double integral form, we obtain

$$\partial D_1(\alpha,\beta,z)/\partial z|_{z=H-h} = -\frac{4}{\pi^2}\sum_{n=1}^{\infty}[a_nR_{1n}+b_nS_{1n}+c_nT_{1n}], \tag{21a}$$

$$\partial D_2(\alpha,\beta,z)/\partial z|_{z=H-h} = -\frac{4}{\pi^2}\sum_{n=1}^{\infty}[a_nR_{2n}+b_nS_{2n}+c_nT_{2n}], \tag{21b}$$

$$D_3(\alpha,\beta,H-h) = -\frac{4}{\pi^2}\sum_{n=1}^{\infty}[a_nR_{3n}+b_nS_{3n}+c_nT_{3n}], \tag{21c}$$

$$D_1(\alpha,\beta,-h) = -\frac{4}{\pi^2}\sum_{n=1}^{\infty}[a_nR_{4n}+b_nS_{4n}+c_nT_{4n}], \tag{21d}$$

$$D_2(\alpha,\beta,-h) = -\frac{4}{\pi^2}\sum_{n=1}^{\infty}[a_nR_{5n}+b_nS_{5n}+c_nT_{5n}], \tag{21e}$$

$$D_3(\alpha,\beta,-h) = -\frac{4}{\pi^2}\sum_{n=1}^{\infty}[a_nR_{6n}+b_nS_{6n}+c_nT_{6n}]. \tag{21f}$$

Then, the 6 linear algebraic equations in Eq. (20) are easy to solve via a simple matrix inverse,

$$\boldsymbol{C}_{AB} = \begin{pmatrix} \partial\boldsymbol{M}_1(\alpha,\beta,z)/\partial z|_{z=H-h} \\ \partial\boldsymbol{M}_2(\alpha,\beta,z)/\partial z|_{z=H-h} \\ \boldsymbol{M}_3(\alpha,\beta,H-h) \\ \boldsymbol{M}_1(\alpha,\beta,-h) \\ \boldsymbol{M}_2(\alpha,\beta,-h) \\ \boldsymbol{M}_3(\alpha,\beta,-h) \end{pmatrix}^{-1} \cdot \begin{pmatrix} \partial D_1(\alpha,\beta,z)/\partial z|_{z=H-h} \\ \partial D_2(\alpha,\beta,z)/\partial z|_{z=H-h} \\ D_3(\alpha,\beta,H-h) \\ D_1(\alpha,\beta,-h) \\ D_2(\alpha,\beta,-h) \\ D_3(\alpha,\beta,-h) \end{pmatrix}. \tag{22}$$

Thus, $\boldsymbol{C}_{AB}=(A_a,A_b,A_c,B_a,B_b,B_c)^{\mathrm{T}}$ is successfully eliminated by being represented as a function of a_n, b_n, and c_n, and the upper and bottom boundary conditions are satisfied analytically. Then, the velocities u_b, v_b, and w_b are available by substituting the $\boldsymbol{C}_{AB}$ expressions of Eq. (22) into Eq. (11) to obtain the functions $D_1(\alpha,\beta,z)$, $D_2(\alpha,\beta,z)$, and $D_3(\alpha,\beta,z)$,

$$D_1(\alpha,\beta,z) = -\frac{4}{\pi^2}\sum_{n=1}^{\infty}\left[a_n\Lambda_n^{11}+b_n\Lambda_n^{12}+c_n\Lambda_n^{13}\right], \tag{23a}$$

$$D_2(\alpha,\beta,z) = -\frac{4}{\pi^2}\sum_{n=1}^{\infty}\left[a_n\Lambda_n^{21}+b_n\Lambda_n^{22}+c_n\Lambda_n^{23}\right], \tag{23b}$$

$$D_3(\alpha,\beta,z) = -\frac{4}{\pi^2}\sum_{n=1}^{\infty}\left[a_n\Lambda_n^{31}+b_n\Lambda_n^{32}+c_n\Lambda_n^{33}\right], \tag{23c}$$

where the detailed expressions of Λ_n^{ij} ($i,j=1,2,3$) in Eq. (23) are summarized in Appendix C.

With the knowledge of $D_1(\alpha,\beta,z)$, $D_2(\alpha,\beta,z)$, and $D_3(\alpha,\beta,z)$, the disturbance $\boldsymbol{u}_b$ produced by the upper and bottom boundaries can be obtained by solving the integral in Eq. (10) and can be given in the same form of $\boldsymbol{u}_s$ as

$$u_b = \sum_{n=1}^{\infty}(a_nA_n'^u+b_nB_n'^u+c_nC_n'^u), \tag{24a}$$

$$v_b = \sum_{n=1}^{\infty}(a_nA_n'^v+b_nB_n'^v+c_nC_n'^v), \tag{24b}$$

$$w_b = \sum_{n=1}^{\infty}(a_nA_n'^w+b_nB_n'^w+c_nC_n'^w), \tag{24c}$$

where

$$\begin{pmatrix} A_n'^u & B_n'^u & C_n'^u \end{pmatrix} = -\frac{4}{\pi^2}\int_0^\infty\int_0^\infty \begin{pmatrix} \Lambda_n^{11} & \Lambda_n^{12} & \Lambda_n^{13} \end{pmatrix} \times \cos\alpha x\cos\beta y\mathrm{d}\alpha\mathrm{d}\beta, \tag{25a}$$

$$\begin{pmatrix} A_n'^v & B_n'^v & C_n'^v \end{pmatrix} = -\frac{4}{\pi^2}\int_0^\infty\int_0^\infty \begin{pmatrix} \Lambda_n^{21} & \Lambda_n^{22} & \Lambda_n^{23} \end{pmatrix} \times \sin\alpha x\sin\beta y\mathrm{d}\alpha\mathrm{d}\beta, \tag{25b}$$

$$\begin{pmatrix} A_n'^w & B_n'^w & C_n'^w \end{pmatrix} = -\frac{4}{\pi^2}\int_0^\infty\int_0^\infty \begin{pmatrix} \Lambda_n^{31} & \Lambda_n^{32} & \Lambda_n^{33} \end{pmatrix} \times \sin\alpha x\cos\beta y\mathrm{d}\alpha\mathrm{d}\beta. \tag{25c}$$

The integrals in Eq. (25) must be performed numerically. First, the integral variables (α,β) in Eq. (25) are transformed to (κ,γ) by making $\alpha=\kappa\cos\gamma$ and $\beta=\kappa\sin\gamma$ ($\kappa\geq 0$, $0\leq\gamma\leq\pi/2$ and $\mathrm{d}\alpha\mathrm{d}\beta=\kappa\mathrm{d}\kappa\mathrm{d}\gamma$),

$$\left(A_n'^u \quad B_n'^u \quad C_n'^u\right) = -\frac{4}{\pi^2}\int_0^\infty\int_0^{\pi/2} \kappa\left(\Lambda_n^{11} \quad \Lambda_n^{12} \quad \Lambda_n^{13}\right) \times \cos(\kappa x\cos\gamma)\cos(\kappa y\sin\gamma)\mathrm{d}\gamma\mathrm{d}\kappa, \quad (26a)$$

$$\left(A_n'^v \quad B_n'^v \quad C_n'^v\right) = -\frac{4}{\pi^2}\int_0^\infty\int_0^{\pi/2} \kappa\left(\Lambda_n^{21} \quad \Lambda_n^{22} \quad \Lambda_n^{23}\right) \times \sin(\kappa x\cos\gamma)\sin(\kappa y\sin\gamma)\mathrm{d}\gamma\mathrm{d}\kappa, \quad (26b)$$

$$\left(A_n'^w \quad B_n'^w \quad C_n'^w\right) = -\frac{4}{\pi^2}\int_0^\infty\int_0^{\pi/2} \kappa\left(\Lambda_n^{31} \quad \Lambda_n^{32} \quad \Lambda_n^{33}\right) \times \sin(\kappa x\cos\gamma)\cos(\kappa y\sin\gamma)\mathrm{d}\gamma\mathrm{d}\kappa. \quad (26c)$$

After transformation, the inner integral of Λ_n^{ij} $(i,j=1,2,3)$ with respect to γ could be performed analytically according to formulae (D1)–(D7) listed in Appendix D by referring to Erdélyi *et al.* (1954). The results ζ_n^{ij} $(i, j = 1, 2, 3)$ of the inner integrals are listed in Appendix D and are reorganized as polynomials of the product of three parts, one of the G_{11}–I_6 functions [Appendix C, (C10)–(C31)], one of the F_1–F_4 functions [Appendix B, (B28)–(B36)], and one of the Bessel functions of the first kind [Appendix D, (D1)–(D7)], which comes from the integral with respect to γ,

$$\left(A_n'^u \quad B_n'^u \quad C_n'^u\right) = -\frac{4}{\pi^2}\int_0^\infty \kappa\left(\zeta_n^{11} \quad \zeta_n^{12} \quad \zeta_n^{13}\right)\mathrm{d}\kappa, \quad (27a)$$

$$\left(A_n'^v \quad B_n'^v \quad C_n'^v\right) = -\frac{4}{\pi^2}\int_0^\infty \kappa\left(\zeta_n^{21} \quad \zeta_n^{22} \quad \zeta_n^{23}\right)\mathrm{d}\kappa, \quad (27b)$$

$$\left(A_n'^w \quad B_n'^w \quad C_n'^w\right) = -\frac{4}{\pi^2}\int_0^\infty \kappa\left(\zeta_n^{31} \quad \zeta_n^{32} \quad \zeta_n^{33}\right)\mathrm{d}\kappa. \quad (27c)$$

These integrand functions ζ_n^{ij} $(i, j = 1, 2, 3)$ must be handled numerically. Functions F_1, F_{21}, F_{22}, F_3, and F_4 can be replaced by forms of simple multiplication of the κ's exponential function and its power function at certain values. The simplified forms of F_1–F_4 are listed in Appendix B. The G_{11}–I_6 functions and the first kind Bessel functions are expanded via the Taylor series for small values of κ and approximated by their asymptotic functions (Abramowitz and Stegun, 1970) for large values of κ, and the breaking point of small values and large values for κ is set to $2/H$. After approximation of these functions, the integrals in Eq. (27) can be solved analytically. Hence, the velocity $\boldsymbol{u}_b$ is easy to obtain through Eq. (24), and the complete solution of the velocities in Eq. (28) is obtained in the form of simple algebraic expressions of the following variables: water depth H, distance h from the particle center to the bottom, position coordinates (r, θ, φ), and a group of remaining unknown constants a_n, b_n, and c_n,

$$u = u_\infty + \sum_{n=1}^{\infty}\left[a_n(A_n^u + A_n'^u) + b_n(B_n^u + B_n'^u) + c_n(C_n^u + C_n'^u)\right], \quad (28a)$$

$$v = v_\infty + \sum_{n=1}^{\infty}\left[a_n(A_n^v + A_n'^v) + b_n(B_n^v + B_n'^v) + c_n(C_n^v + C_n'^v)\right], \quad (28b)$$

$$w = w_\infty + \sum_{n=1}^{\infty}\left[a_n(A_n^w + A_n'^w) + b_n(B_n^w + B_n'^w) + c_n(C_n^w + C_n'^w)\right]. \quad (28c)$$

2. Determination of unknown constants (a_n, b_n, c_n) for u_s

After $\boldsymbol{u}_b$ is solved, the remaining unknowns u, v, and w are the constants a_n, b_n, and c_n in Eq. (28). These constants can be obtained through $\boldsymbol{u}$ satisfying the sphere surface boundary condition [Eq. (2c)]. According to Eq. (28), the exact solution of u, v, and w requires three infinite arrays of unknown constants a_n, b_n, and c_n $(n = 1, 2, 3, \ldots)$, so the converged collocation technique (Ganatos *et al.*, 1980 and O'Brien, 1968) of applying the non-slip condition in Eq. (2c) to a finite number (N) of discrete points on the sphere is used, and a corresponding truncation $(n = 1, 2, \ldots, N)$ is made to the infinite series of u, v, and w in Eq. (28). It is convergent because the terms (A_n^i, B_n^i, C_n^i) and $(A_n'^i, B_n'^i, C_n'^i$, and $i = u, v, w)$ in the series decay as n increases. When the non-slip boundary conditions are applied to the N points on the sphere, $3N$ linear algebraic equations are set up; therefore, the determination of the $3N$ constants a_n, b_n, c_n $(n = 1, 2, \ldots, N)$ can be achieved.

III. RESULTS AND DISCUSSION

A. Convergence test

Before being applied to the drag force and torque calculation, the convergence test of the present solution is implemented in this section. The values of the nondimensional drag force and torque are chosen to show the convergent process.

The present bounded drag force of the sphere $F_x = 4\pi\mu a_1$ in Eq. (15a) is nondimensionalized using Stokes' drag law $F_{\text{Stokes}} = 6\pi\mu a\, u_\infty|_{z=0}$ of an unbounded fluid to a nondimensional constant f_x^*,

$$f_x^* = \frac{F_x}{F_{\text{Stokes}}} = -\frac{2a_1}{3a\, u_\infty|_{z=0}}, \quad (29)$$

where, $u_\infty|_{z=0}$ is the streamwise velocity of the external driving flow $\boldsymbol{u}_\infty$ at the height of the sphere center and can be written as $u_\infty|_{z=0} = u_m\left[2h/H - (h/H)^2\right]$ according to Eq. (4b) for a laminar open channel flow, where u_m is the maximum velocity of u_∞, h/H is the ratio of the lower interval and water depth, and a_1 is a constant to be determined.

The magnitude of the torque acting on the sphere is generally considered to be positively related to the velocity shear rate of the external fields, such as the velocity shear rates of $\boldsymbol{u}_\infty$ and $\boldsymbol{u}_b$ evaluated at the center of the sphere in the present problem. Generally, scalar linearly related to the shear rate of $\boldsymbol{u}_\infty$ or $\boldsymbol{u}_b$ is used to nondimensionalize the torque. However, these two scalars are both inappropriate because the former is close to 0 when the sphere is near the top and the latter is unknown beforehand; therefore, a simple characteristic scalar $8\pi\mu a^2 u_m$ with the dimensions of torque but no physical meaning related to torque is adopted. According to the torque expressions in Eq. (15b), the nondimensional torque t_y^* is written as

$$t_y^* = \frac{T_y}{8\pi\mu a^2 u_m} = -\frac{c_1}{a^2 u_m}, \quad (30)$$

where c_1 is the constant to be determined.

An increasing number of points arranged on the sphere surface under the condition of $H = 20a$ are considered (Tables I and II). Since the problem is symmetric about the plane $y = 0$, only the hemisphere of $\theta \in (0, \frac{\pi}{2}) \cup \left(\frac{\pi}{2}, \pi\right)$ and a constant φ is chosen to uniformly locate these points. Different h/a and $\frac{(H-h)}{a}$ situations are considered. When the target position is distant from the boundaries, the method converges quickly. By contrast, when the sphere is quite close to the boundaries and the singularity arises, it is difficult to converge and fluctuations occur due to the truncations made by the collocation method, the replacement of infinite series of $\boldsymbol{u}_s$ and double integrals of $\boldsymbol{u}_b$ by finite series becomes defective in this limiting case. On the whole, a number of $N = 16$ is enough.

To check our solution more carefully, the velocity results calculated by the present solution are compared with that by a N-S equation based numerical model. The velocities in the plane $y = 0$ are chosen to show the comparison. The case ($H/a = 10$ with $h/a = 2.0$) is considered. The numerical result is simulated by simpleFoam of OpenFOAM (Weller *et al.*, 1998), the numerical domain is $100a$, $60a$, and $10a$ in the x, y, and z directions, respectively, the grid size is gradually refined to $a/16$ near the sphere surface. These domain and grid resolution are sufficient according to Zeng *et al.* (2005). The flow is driven by a velocity inlet as described by Eq. (4b). The no-slip condition is applied to the bottom plane and the sphere surface; the free-slip condition is applied to the top plane and the lateral boundaries in the y direction and outlet to the downstream boundary.

The results for $H/a = 10$ with $h/a = 2.0$ are plotted in Fig. 2. The calculated results and the simulated results are consistent with each other. For the calculated results, the no-slip condition on the sphere surface is perfectly satisfied by the collocation method. The no-slip bottom and the free-slip top boundary conditions are analytical satisfied originally as described by Eqs. (16)–(26). However, the integrals in Eq. (27) of $\boldsymbol{u}_b$ cannot be solved analytically after applying the bottom and top boundary conditions; several subfunctions of these integrands are replaced by their piecewise approximations to get the semi-analytical solution of $\boldsymbol{u}_b$. This approximation process caused small deviations from the original boundary conditions and is responsible for the non-zero values at the bottom boundary in Fig. 2(a).

B. Drag force results

A series of convergent results of the nondimensional drag force f_x^* defined by Eq. (29) for a stationary sphere immersed in a laminar open channel flow are presented in Table III and are plotted correspondingly in Fig. 3.

As shown in Fig. 3(a), for each fixed $(H - h)/a$ corresponding to a column in Table III, f_x^* increases monotonically as h/a decreases. This phenomenon indicates that the bottom wall has an incremental effect on the hydrodynamic drag of a sphere close to it; the closer the sphere is, the stronger the incremental effect is. When $(H - h)/a$ is large enough, as seen in the last column of Table III, where $f_x^* = 1.0$, in which there is a zero boundary effect on the nondimensional drag force, the influence of the top surface can be ignored, and the bottom wall is the only impact factor for f_x^*. We find that the bottom wall produces more than 3% of the impact on the drag force when $h/a < 20$ and less than 1% of the impact when $h/a > 50$.

TABLE I. Convergence of f_x^* under the condition of $H = 20a$.

	h/a								$(H-h)/a$				
N	1.0	1.003	1.125	1.251	1.5	2	3	5	5	3	2	1.5	1.251
2	1.741	1.737	1.626	1.546	1.44	1.321	1.21	1.125	1.031	0.981	0.917	0.857	0.816
4	1.630	1.628	1.570	1.517	1.432	1.322	1.210	1.126	1.032	0.984	0.925	0.873	0.836
6	1.677	1.675	1.602	1.540	1.446	1.327	1.212	1.126	1.032	0.984	0.926	0.873	0.837
8	1.687	1.685	1.607	1.543	1.447	1.327	1.212	1.126	1.032	0.984	0.926	0.873	0.836
10	1.690	1.688	1.609	1.544	1.447	1.328	1.212	1.126	1.032	0.984	0.926	0.873	0.836
12	1.690	1.688	1.609	1.544	1.447	1.328	1.212	1.126	1.032	0.984	0.926	0.874	0.836
14	1.689	1.687	1.610	1.544	1.447	1.328	1.212	1.126	1.032	0.984	0.926	0.874	0.836
16	1.687	1.686	1.602	1.544	1.447	1.328	1.212	1.126	1.032	0.984	0.926	0.874	0.836

TABLE II. Convergence of t_y^* under the condition of $H = 20a$. The italicized values in the table represent the negative values.

	h/a								$(H-h)/a$				
N	1.0	1.003	1.125	1.251	1.5	2	3	5	5	3	2	1.5	1.251
2	0.565	0.565	0.531	0.491	0.416	0.303	0.186	0.097	*0.008*	*0.032*	*0.077*	*0.126*	*0.163*
4	0.954	0.951	0.840	0.753	0.628	0.469	0.305	0.171	0.013	*0.024*	*0.074*	*0.127*	*0.169*
6	0.922	0.920	0.824	0.745	0.625	0.468	0.305	0.171	0.013	*0.025*	*0.076*	*0.134*	*0.181*
8	0.902	0.899	0.812	0.736	0.619	0.465	0.304	0.171	0.013	*0.025*	*0.075*	*0.132*	*0.178*
10	0.897	0.895	0.810	0.735	0.619	0.465	0.304	0.171	0.013	*0.025*	*0.076*	*0.133*	*0.179*
12	0.898	0.896	0.810	0.735	0.619	0.465	0.304	0.171	0.013	*0.025*	*0.076*	*0.133*	*0.179*
14	0.899	0.897	0.812	0.736	0.619	0.465	0.304	0.171	0.013	*0.025*	*0.076*	*0.133*	*0.179*
16	0.898	0.903	0.812	0.736	0.618	0.465	0.304	0.171	0.013	*0.025*	*0.076*	*0.135*	*0.179*

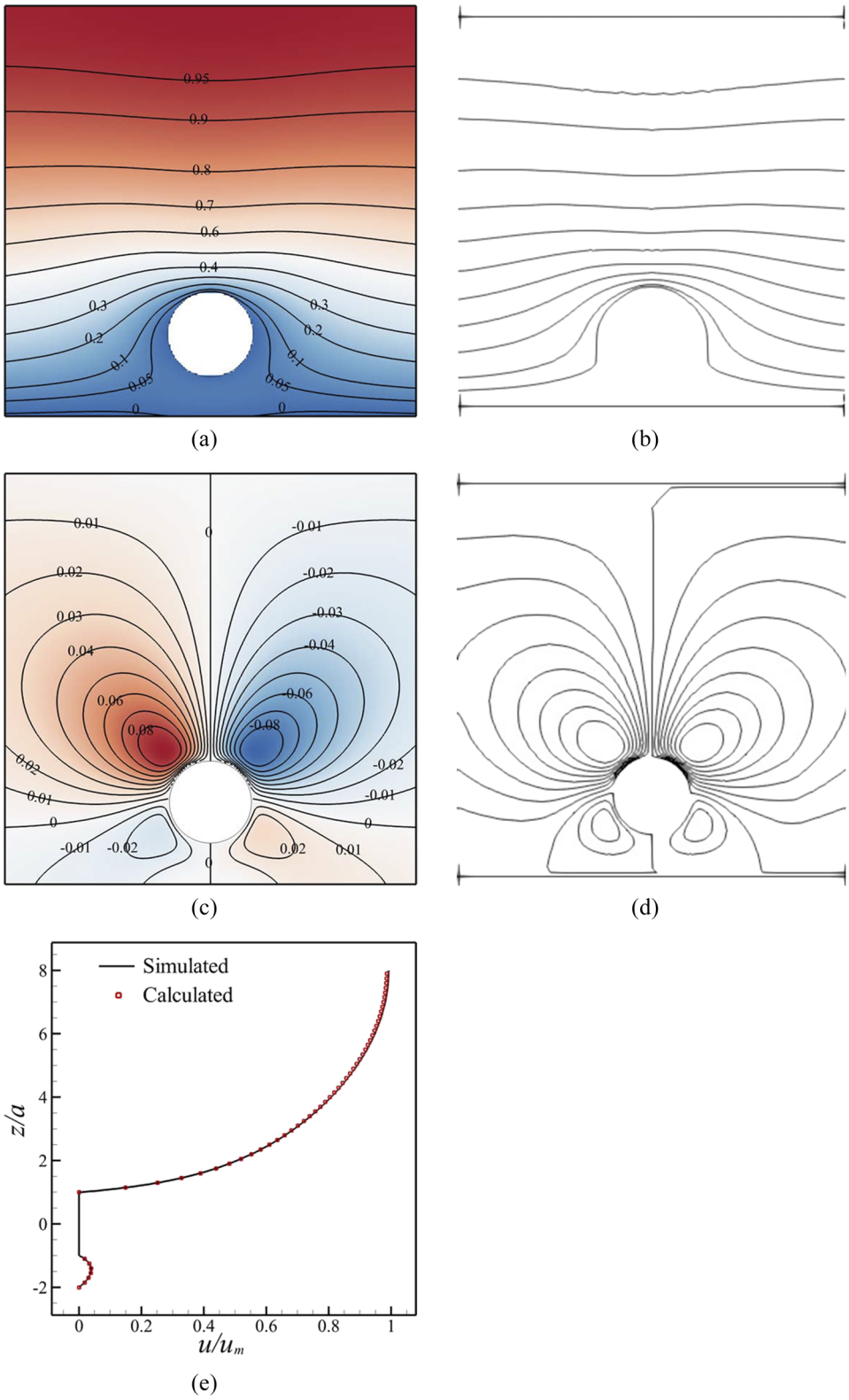

FIG. 2. The calculated and the simulated velocity contours in the plane $y = 0$ for $H/a = 10$ and $h/a = 2.0$ are shown with the same contour legend for the calculated and the simulated values: (a) the calculated u, (b) the simulated u, (c) the calculated w, and (d) the simulated w. The bottom figure (e) shows the comparison of the calculated u and the simulated u along the vertical line across the sphere ($x = -a/40$ and $y = 0$). The singularity occurs at $\theta = 0$ and π, so the vertical line is not accurately placed across the sphere center but at $x = -a/40$.

In contrast to the incremental effect from the bottom wall, the slip top mainly shows a decremental effect on the drag of the sphere. In Fig. 3(b), for the sphere in a channel with a fixed height H, f_x^* tends to decrease when the sphere is closer to the top surface. When the influence of the bottom wall is excluded (e.g., the last row in Table III when h/a is large enough), the slip top produces an impact of greater than 3% on the drag force when $(H - h)/a \leq 10$ and less than 0.5% impact when $(H - h)/a > 50$.

For a sphere in an open channel of any height, the nondimensional drag f_x^* decreases as the sphere location changes from the bottom wall to the top surface [Fig. 3(b)]. For all height conditions that satisfy $H > 5.6a$ [i.e., the distance from the sphere center to the top surface is $(1 - 0.82)H > a$], when

TABLE III. Variation of the nondimensional drag force f_x^* for a stationary sphere immersed in a laminar open channel flow with h/a and $(H-h)/a$, which are, respectively, the nondimensional lower interval between the sphere center and the bottom wall and the nondimensional upper interval from the sphere center to the upper surface.

	$(H-h)/a$									
h/a	1.001	1.251	1.5	2.0	3.0	5.0	10.0	20.0	50.0	1000
1.0	1.813	1.792	1.799	1.773	1.722	1.688	1.683	1.687	1.691	1.697
1.003	1.812	1.792	1.798	1.775	1.724	1.690	1.684	1.696	1.690	1.703
1.251	1.554	1.613	1.625	1.621	1.584	1.551	1.541	1.544	1.547	1.549
1.5	1.435	1.493	1.516	1.519	1.491	1.459	1.446	1.447	1.451	1.452
2.0	1.283	1.338	1.369	1.388	1.374	1.346	1.329	1.328	1.330	1.331
3.0	1.112	1.170	1.209	1.244	1.253	1.235	1.216	1.211	1.212	1.213
5.0	0.965	1.021	1.062	1.110	1.143	1.146	1.131	1.123	1.122	1.123
10.0	0.847	0.897	0.937	0.989	1.038	1.067	1.070	1.063	1.059	1.059
20.0	0.786	0.832	0.868	0.918	0.971	1.012	1.033	1.034	1.030	1.029
50.0	0.749	0.791	0.825	0.871	0.923	0.967	0.999	1.012	1.014	1.011
100	0.737	0.778	0.810	0.855	0.906	0.949	0.983	1.000	1.007	1.006
500	0.731	0.767	0.798	0.842	0.891	0.934	0.968	0.986	0.997	1.001
1000	0.723	0.765	0.795	0.840	0.889	0.932	0.966	0.984	0.995	1.001

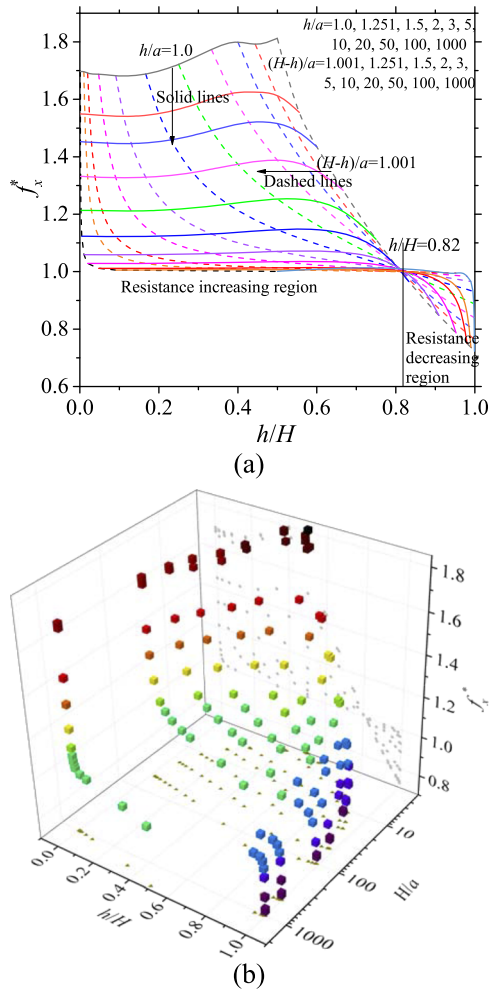

FIG. 3. Nondimensional drag force f_x^* for a stationary sphere immersed in a laminar open channel flow at different locations: (a) f_x^* plotted versus h/H, the solid lines are results of various nondimensional lower intervals h/a, the dashed lines are results of various nondimensional upper intervals $(H-h)/a$; (b) f_x^* plotted versus h/H for various nondimensional water depths H/a. h/H is the height ratio of the sphere center and the water depth in an open channel, and the sphere radius a is chosen as the characteristic length for nondimensionalization.

the sphere locates at approximately 0.82 times the height of the open channel ($h/H = 0.82$), its drag force is approximately the same magnitude of that in an unbounded field ($f_x^* \approx 1.0$). This plane $h = 0.82H$ divides the entire channel into two parts: the resistance increasing region (RI region: $h < 0.82H$) with f_x^* greater than 1.0 and the resistance decreasing region (RD region: $h > 0.82H$) with f_x^* less than 1.0. In the RI region, the incremental effect of the bottom wall dominates, while in the RD region, the decremental effect of the slip surface dominates. For regions in $(H-h)/a > 10 \cap h/a > 20$, $|f_x^* - 1.0| < 0.03$, the effect of both bounding surfaces is weak, and the drag force is almost equal to that of the unbounded condition, as described by Stokes' drag law.

C. Torque results

The nondimensional torque t_y^* calculated using Eq. (30) at different locations in a laminar open channel flow is partly displayed in Table IV and plotted in Fig. 4. There is an obvious gradual change from positive to zero, and then to negative torque values, as seen in Fig. 4(a), as the location of the sphere center (h/H) increases from 0 to 1, where the magnitude of the torque increases as the sphere center is closer to the bottom or top boundary. Away from both boundaries of the open channel, the magnitude of torque is small.

For each fixed water depth (H/a), as shown in Fig. 4(b), the region of positive torque values is always larger than that for negative torque values, the zero value always occurs above the half depth of the channel, and the larger the water depth is, the larger the positive region proportion is. For a large water depth, most of the positive region away from both boundaries has quite small values.

D. Special case of *h*/*H* converging to zero and *H* tending to infinity

For a laminar open channel flow $\boldsymbol{u}_\infty$, the shear rate of the streamwise velocity is given as

TABLE IV. Variation of the nondimensional torque t_y^* for a stationary sphere immersed in a laminar open channel flow with nondimensional intervals h/a from the bottom wall and $(H-h)/a$ from the top surface. The italicized values in the table represent the negative values.

	$(H-h)/a$										
h/a	1.001	1.251	1.5	2.0	3.0	5.0	10.0	20.0	50.0	100	1000
1.0	0.079	0.126	0.156	0.181	0.167	0.126	0.076	0.042	0.018	0.009	0.001
1.003	0.080	0.126	0.156	0.181	0.167	0.127	0.076	0.042	0.018	0.009	0.001
1.251	0.024	0.089	0.128	0.158	0.154	0.121	0.075	0.042	0.018	0.009	0.001
1.5	*0.012*	0.059	0.099	0.134	0.139	0.114	0.073	0.042	0.018	0.009	0.001
2.0	*0.055*	0.010	0.052	0.094	0.112	0.100	0.068	0.041	0.018	0.009	0.001
3.0	*0.095*	*0.041*	*0.004*	0.042	0.072	0.076	0.059	0.038	0.018	0.009	0.001
5.0	*0.118*	*0.076*	*0.044*	*0.002*	0.031	0.047	0.044	0.032	0.016	0.009	0.001
10.0	*0.123*	*0.089*	*0.064*	*0.030*	*0.001*	0.016	0.024	0.022	0.014	0.008	0.001
20.0	*0.120*	*0.089*	*0.067*	*0.038*	*0.014*	0.001	0.010	0.012	0.010	0.007	0.001
50.0	*0.116*	*0.087*	*0.067*	*0.040*	*0.018*	*0.006*	0.001	0.004	0.005	0.004	0.001
100	*0.114*	*0.086*	*0.065*	*0.039*	*0.019*	*0.007*	*0.001*	0.001	0.002	0.002	0.001
500	*0.113*	*0.085*	*0.065*	*0.039*	*0.019*	*0.007*	*0.002*	0.000	0.000	0.000	0.000
1000	*0.111*	*0.085*	*0.057*	*0.039*	*0.018*	*0.007*	*0.002*	0.000	0.000	0.000	0.000

$$\frac{\mathrm{d}u_\infty}{\mathrm{d}z} = \frac{2u_m}{H}\left(1 - \frac{z+h}{H}\right). \tag{31}$$

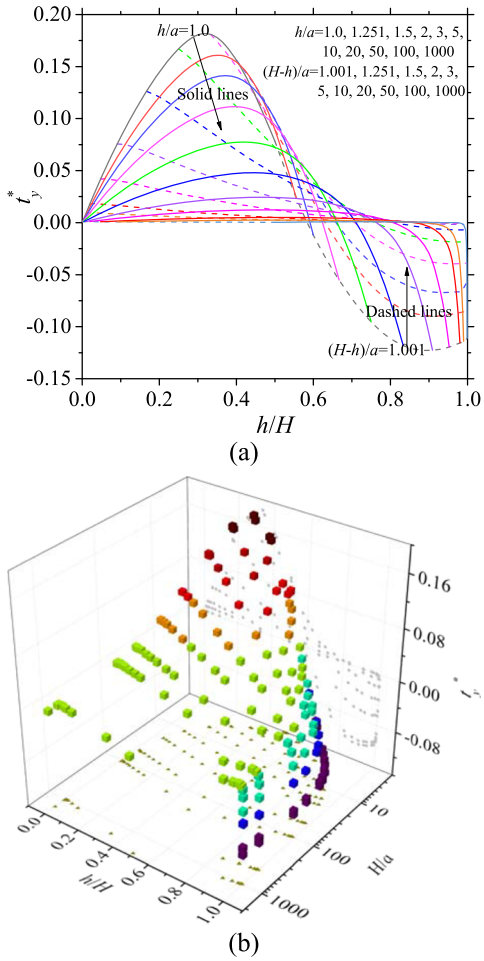

FIG. 4. Nondimensional torque t_y^* on a stationary sphere immersed in a laminar open channel flow at different locations: (a) t_y^* plotted versus h/H; the solid lines are the results of various nondimensional lower interval values h/a, and the dashed lines are the results of various nondimensional upper interval values $(H-h)/a$; (b) t_y^* plotted versus h/H for various nondimensional water depths H/a.

When the upper surface goes to infinity ($H \to +\infty$) and the sphere is at a finite height above the bottom wall ($h/H \to 0$), the shear rate of the laminar open channel flow evaluated at the sphere center ($z = 0$) will approach a constant $2u_m/H$; thus, the external flow in the region, where the sphere and the bottom wall interact, could be regarded as a linear shear flow. Under this condition, the data results of the present open channel flow solution approach those of the linear shear flow solution by Goldman *et al.* (1967).

When normalized with a constant shear rate $2u_m/H$, the nondimensional force and the torque of a stationary sphere are, respectively, calculated as

$$f_x^{s^*} = \frac{F_x}{6\pi\mu a h} \times \frac{1}{2u_m/H}, \tag{32a}$$

$$t_y^{s^*} = \frac{T_y}{4\pi\mu a^3} \times \frac{1}{2u_m/H}, \tag{32b}$$

where $f_x^{s^*}$ and $t_y^{s^*}$ are the nondimensional forms of F_x and T_y.

A series of progressively decreasing values of h/a and final converged values of $h/a = 0$ are considered. The results listed in Tables V and VI show an apparent convergent process of the drag force and torque, respectively, as h/H approaches 0 (H approaches $+\infty$ and h is finite). The convergent data results are consistent with those given in Table I of Goldman *et al.* (1967). The present solution is solvable even at $h/a = 1.0$, and the calculated nondimensional drag f_x^{s*} (which equals 1.7106) shows a deviation of less than 0.6% compared to the analytical result 1.7009 of Leighton and Acrivos (1985) and the extrapolation result 1.7005 of Goldman *et al.* (1967). The nondimensional torque t_y^{s*} (Table VI), which is more sensitive to a change in the shear rate of the flow than the drag is, shows a larger deviation compared to the nondimensional drag when $h/a = 1.0$, but the deviation is still less than 1%. For $h/a \geq 1.128$, the present results (Tables V and VI) show perfect consistency with the results of Goldman *et al.* (1967). For $h/a < 1.05$, the largest deviation of f_x^{s*} (0.62%) and t_y^{s*} (2.0%) from the results of Goldman *et al.* (1967) occurred at

TABLE V. Nondimensional drag forces f_x^{s*} on a stationary sphere in proximity to a wall with various nondimensional distances h/a. The calculated results are compared to the results of Goldman *et al.* (1967).

	h/H					
h/a	1.0×10^{-2}	1.0×10^{-3}	1.0×10^{-4}	1.0×10^{-6}	0	(Goldman)
1.0	1.685	1.696	1.711	1.711	1.711	1.701
1.003	1.694	1.703	1.703	1.703	1.703	1.698
1.045	1.657	1.664	1.659	1.659	1.660	1.668
1.128	1.603	1.615	1.616	1.616	1.616	1.616
1.543	1.432	1.438	1.439	1.439	1.439	1.439
2.352	1.272	1.277	1.278	1.278	1.278	1.278
3.762	1.161	1.167	1.167	1.167	1.167	1.167
10.068	1.053	1.058	1.059	1.059	1.059	1.059
100	1.001	1.005	1.006	1.006	1.006	
1 000	0.996	1.000	1.001	1.001	1.001	
10 000	0.995	1.000	1.000	1.000	1.000	
$+\infty$						1.000

TABLE VI. Nondimensional torques t_y^{s*} on a stationary sphere in proximity to a wall with a nondimensional distance h/a. The results calculated are compared to the results of Goldman *et al.* (1967).

	h/H					
h/a	1.0×10^{-2}	1.0×10^{-3}	1.0×10^{-4}	1.0×10^{-6}	0	(Goldman)
1.0	0.918	0.929	0.938	0.938	0.938	0.944
1.003	0.930	0.935	0.936	0.936	0.936	0.944
1.045	0.926	0.933	0.929	0.929	0.929	0.948
1.128	0.936	0.954	0.955	0.956	0.956	0.954
1.543	0.962	0.971	0.972	0.972	0.972	0.974
2.352	0.980	0.989	0.990	0.990	0.990	0.990
3.762	0.987	0.996	0.997	0.997	0.997	0.997
10.068	0.990	0.999	1.000	1.000	1.000	1.000
100	0.990	0.999	1.000	1.000	1.000	
1000	0.990	0.999	1.000	1.000	1.000	
$+\infty$						1.000

$h/a = 1.0$ (Table V) and $h/a = 1.045$ (Table VI), respectively. This deviation is caused by the piecewise approximations made to the integrand in Eq. (27) to solve for $\boldsymbol{u}_b$ after applying the bottom and top boundary conditions. When the sphere is quite close to the boundary, this deviation is no longer negligible. In general, these comparisons indicate good accuracy of the present solution.

According to results of progressively decreasing h/a in Tables V and VI, the values for $h/H = 0.01$ show a maximum difference of approximately 1.5% for f_x^{s*} and approximately 2% for t_y^{s*} compared to the convergent results; when $h/H = 0.001$, the difference dampens to less than 1% for both f_x^{s*} and t_y^{s*}. Hence, the drag force and torque rules for a sphere in an open channel flow of $h/H \le 0.001$ are almost the same as these properties near a single wall in a linear shear flow.

E. Discussion

In this section, the effect of the bottom wall and the slip top on the drag force and torque of the sphere is discussed. To make this clear, we plot velocity $\boldsymbol{u}$ by Eq. (28) and its three components $\boldsymbol{u}_\infty$ (4), $\boldsymbol{u}_s$ (5) and (6), and $\boldsymbol{u}_b$ (24), separately (Fig. 5) for the case of a water depth $H = 10a$ and $h = 5a$. The vertical distribution of their streamwise velocities (normalized by u_m, the maximum velocity in the streamwise direction) along the vertical straight line through the center of the sphere is also plotted.

According to Sec. II C, we learn that $\boldsymbol{u}_s$ is the direct determinant of drag force and torque of the sphere. The expression of $\boldsymbol{u}_s$ determines the expressions of drag and torque as Eqs. (12)–(15), and the forms of the drag and torque expression are not affected by the external action field felt by the sphere ($\boldsymbol{u}_b$ and $\boldsymbol{u}_\infty$). The magnitudes of the drag force and the torque are determined by the constants a_1 and c_1, respectively, in Eq. (15). These constants are obtained by causing the resultant velocity $\boldsymbol{u}$ satisfy the boundary conditions; the conditions in Eq. (2) are as follows when only its streamwise component is considered:

$$z = -h: \ u_\infty = 0, u_s + u_b = 0, \tag{33a}$$

$$z = H - h: \frac{\partial u_\infty}{\partial z} = 0, \frac{\partial u_s}{\partial z} + \frac{\partial u_b}{\partial z} = 0, \tag{33b}$$

$$r = a: u_\infty + u_s + u_b = 0. \tag{33c}$$

When u_b and u_∞ vary, u_s tends to change its constants correspondingly according to Eq. (33). Since u_∞ is clearly determined in Eq. (4b) and not affected by the existence of the sphere, the main interdependence controlled by the boundary conditions happens between u_s and u_b as Eq. (33) shows. From Fig. 5, we could see the satisfaction of Eq. (33): $u_s|_{z=-h} = -u_b|_{z=-h} < 0$, $\frac{\partial u_s}{\partial z}\Big|_{z=H-h} = -\frac{\partial u_b}{\partial z}\Big|_{z=H-h} > 0$, and $u_s|_{r=a} = -(u_b|_{r=a} + u_\infty|_{r=a}) < 0$. Velocity u_b is born a monotone decreasing field with the ascending position. It is positive ($u_b|_{z=-h}$) at the bottom and has negative gradients $\frac{\partial u_b}{\partial z}\Big|_{z=H-h}$ at the top as Fig. 5(d) shows.

When the sphere is small enough and can be regarded as a point ($a \to 0$) located at $\boldsymbol{r} = 0$ or (x, y, z) = (0, 0, 0), the drag force and the torque of the sphere could be formulated as follows when only the leading orders are considered:

$$F_x = -6\pi\mu a\, u_s|_{(0,0,0)} = 6\pi\mu a\left[u_\infty|_{(0,0,0)} + u_b|_{(0,0,0)}\right], \tag{34a}$$

$$T_y = -8\pi\mu a^3 \frac{\partial u_s}{\partial z}\Big|_{(0,0,0)} = 8\pi\mu a^3\left(\frac{\partial u_\infty}{\partial z}\Big|_{(0,0,0)} + \frac{\partial u_b}{\partial z}\Big|_{(0,0,0)}\right), \tag{34b}$$

$(\,)|_{(0,0,0)}$ represents the value of the variable in parentheses located at (0, 0, 0), then f_x^* and t_y^* could be written as

$$f_x^* = \frac{F_x}{6\pi\mu a\, u_\infty|_{(0,0,0)}} = 1 + \frac{u_b|_{(0,0,0)}}{u_\infty|_{(0,0,0)}}, \tag{35a}$$

$$t_y^* = \frac{T_y}{8\pi\mu a^2 u_m} = \frac{a}{u_m}\left[\frac{\partial u_\infty}{\partial z}\Big|_{(0,0,0)} + \frac{\partial u_b}{\partial z}\Big|_{(0,0,0)}\right]. \tag{35b}$$

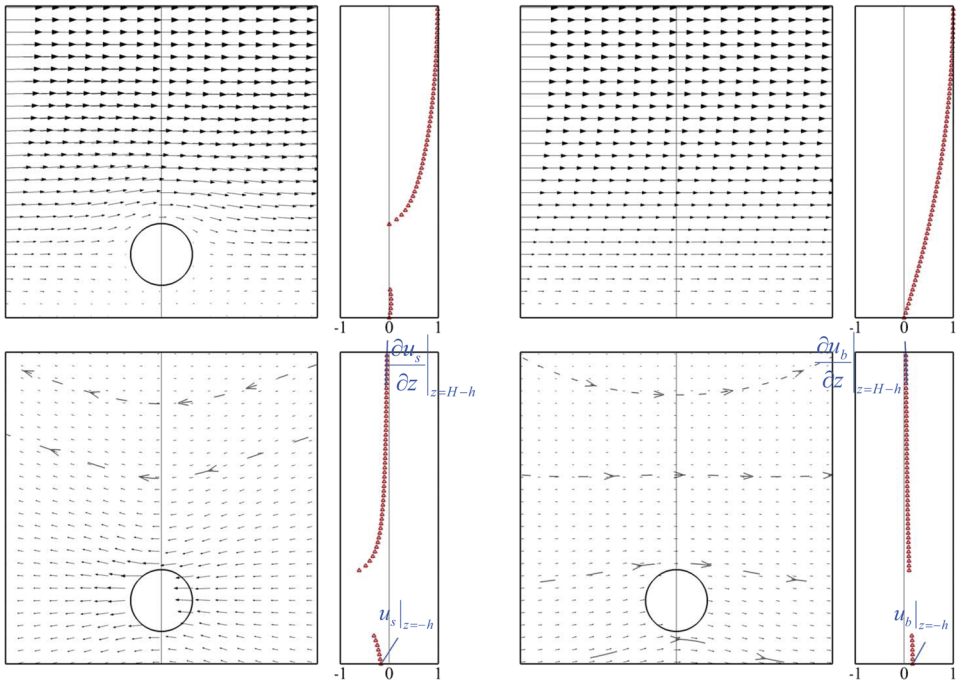

FIG. 5. Velocity vector field in the plane $y = 0$ and their vertical distributions of streamwise velocity (normalized by u_m which is the maximum velocity of u_∞) along the vertical straight line (z-direction) through the center of sphere of $\boldsymbol{u}$ [(a) left top], $\boldsymbol{u}_\infty$ [(b) right top], $\boldsymbol{u}_s$ [(c) left bottom], $\boldsymbol{u}_b$ [(d) right bottom] for the condition of $H = 10a$, $h = 2a$. $\boldsymbol{u}_b$ should be an external field without occupying space from the sphere according to Eqs. (9) and (10). When transformed to forms in Cartesian coordinates as Eq. (24) by satisfying Eq. (19), values of $\boldsymbol{u}_b$ in the region inside the sphere are abandoned since they make no difference to the drag force and torque of the sphere.

Obviously, the value of f_x^* is closely related to the disturbance $u_b|_{(0,0,0)}$ generated by $\boldsymbol{u}_b$ at the sphere surface since $u_\infty|_{(0,0,0)}$ is known, while t_y^* is determined by two shear rates generated by $\boldsymbol{u}_\infty$ and $\boldsymbol{u}_b$, respectively. When $\boldsymbol{u}_s$ is described by a number of singularities of strength $-q_0\left(u_s|_{(0,0,0)}\right)\boldsymbol{e}_x$, which is equal to $q_0\left(u_\infty|_{(0,0,0)} + u_b|_{(0,0,0)}\right)\boldsymbol{e}_x$, located at ($x$, y, z) = (0, 0, 0). The following expressions then can be obtained according to the bottom and top boundary condition, respectively:

$$\begin{aligned} u_b|_{(0,0,-h)} &= \frac{q_0\left(u_\infty|_{(0,0,0)} + u_b|_{(0,0,0)}\right)}{h}, \\ \left.\frac{\partial u_b}{\partial z}\right|_{(0,0,H-h)} &= -\frac{q_1\left(u_\infty|_{(0,0,0)} + u_b|_{(0,0,0)}\right)}{(H-h)^2}, \end{aligned} \tag{36}$$

where q_0 and q_1 are constant expressions independent of h, $H - h$, and H. It is always true that $q_0 > 0$, $q_1 > 0$, and $u_\infty|_{(0,0,0)} + u_b|_{(0,0,0)} > 0$ for the present problem.

In the following text, we try to analyze why the zero boundary effect of the drag force and the torque show different characteristics. Here $\boldsymbol{u}_b$ is also described by a number of singularities located at (0, 0, 0), whose strength is in proportion to $\left(u_\infty|_{(0,0,0)} + u_b|_{(0,0,0)}\right)\boldsymbol{e}_x$, then we suppose the following relations according to Eq. (36):

$$\begin{aligned} \left.\frac{\partial^n u_b}{\partial z^n}\right|_{(0,0,-h)} &\propto (-1)^n \frac{\left(u_\infty|_{(0,0,0)} + u_b|_{(0,0,0)}\right)}{h^{n+1}}, \\ \left.\frac{\partial^n u_b}{\partial z^n}\right|_{(0,0,H-h)} &\propto (-1)^n \frac{\left(u_\infty|_{(0,0,0)} + u_b|_{(0,0,0)}\right)}{(H-h)^{n+1}}. \end{aligned} \tag{37}$$

Taylor expansions of $u_b|_{(0,0,0)}$ and $\left.\frac{\partial u_b}{\partial z}\right|_{(0,0,H-h)}$ at (0, 0, $-h$) give

$$u_b|_{(0,0,0)} = u_b|_{(0,0,-h)} + \left.\frac{\partial u_b}{\partial z}\right|_{(0,0,-h)} h + \sum_{n=2}^{\infty}\left[\frac{1}{n!}\left.\frac{\partial^n u_b}{\partial z^n}\right|_{(0,0,-h)} h^n\right], \tag{38a}$$

$$\left.\frac{\partial u_b}{\partial z}\right|_{(0,0,-h)} = \left.\frac{\partial u_b}{\partial z}\right|_{(0,0,H-h)} - \sum_{n=2}^{\infty}\left[\frac{1}{(n-1)!}\left.\frac{\partial^n u_b}{\partial z^n}\right|_{(0,0,-h)} H^{n-1}\right]. \tag{38b}$$

By substituting Eq. (38b) into Eq. (38a), we get

$$\begin{aligned} u_b|_{(0,0,0)} = u_b|_{(0,0,-h)} &+ \left.\frac{\partial u_b}{\partial z}\right|_{(0,0,H-h)} h \\ &+ \sum_{n=2}^{\infty}\left[\left.\frac{\partial^n u_b}{\partial z^n}\right|_{(0,0,-h)}\left(\frac{h^n}{n!} - \frac{H^{n-1}h}{(n-1)!}\right)\right]. \end{aligned} \tag{39a}$$

According to Eq. (37), the above expression could be transformed to

$$\frac{u_b|_{(0,0,0)}}{u_\infty|_{(0,0,0)}} = \left(\frac{u_b|_{(0,0,0)}}{u_\infty|_{(0,0,0)}} + 1\right)\frac{1}{h}g\left(\frac{h}{H}\right), \tag{39b}$$

where $g\left(\frac{h}{H}\right) = q_0 - q_1\left(\frac{1}{H/h-1}\right)^2 + \sum_{n=2}^{\infty} q_n(-1)^n\left[\frac{1}{n!} - \frac{1}{(n-1)!}\left(\frac{H}{h}\right)^{n-1}\right]$, q_n ($n = 2, 3, \ldots$) are positive expressions independent of h, $H - h$, and H. Obviously, we have $\frac{u_b|_{(0,0,0)}}{u_\infty|_{(0,0,0)}} = \frac{g(h/H)}{h - g(h/H)}$ according to Eq. (39b), then the nondimensional drag force f_x^* based on Eq. (35a) could be written as

$$f_x^* = 1 + \frac{g(h/H)}{h - g(h/H)}. \tag{40}$$

Therefore, we could tell that f_x^* is mainly controlled by $\frac{h}{a}$ and $\frac{h}{H}$. Moreover, $f_x^* = 1.0$ will always be true when $g(h/H)$

equals 0, which could be obtained at a constant $\frac{h}{H}$ according to Eq. (40). This may explain the phenomenon in Sec. III B that the nondimensional drag force f_x^* always equals 1.0 at a constant value of $\frac{h}{H}$ which does not change with the depth of the channel.

For the shear rate, a Taylor expansion of $\frac{\partial u_b}{\partial z}\big|_{(0,0,0)}$ at $(0, 0, H-h)$ gives

$$\left.\frac{\partial u_b}{\partial z}\right|_{(0,0,0)} = \left.\frac{\partial u_b}{\partial z}\right|_{(0,0,H-h)} + \sum_{n=2}^{\infty}\left[\frac{1}{(n-1)!}\left.\frac{\partial^n u_b}{\partial z^n}\right|_{(0,0,H-h)}(h-H)^{n-1}\right]. \quad (41)$$

By substituting $\left.\frac{\partial u_b}{\partial z}\right|_{(0,0,H-h)} = \frac{q_1(u_\infty|_{(0,0,0)}+u_b|_{(0,0,0)})}{(H-h)^2}$ in Eq. (36), $\frac{u_b|_{(0,0,0)}}{u_\infty|_{(0,0,0)}} = \frac{g(h/H)}{h-g(h/H)}$ from Eq. (40), and $u_\infty|_{(0,0,0)} = u_m\left(2\frac{h}{H}-\frac{h^2}{H^2}\right)$ from Eq. (4b), and applying the relations in Eq. (37), the above equation could be written as

$$\left.\frac{\partial u_b}{\partial z}\right|_{z=0} = Q\frac{u_m h\left(2\frac{h}{H}-\frac{h^2}{H^2}\right)}{(H-h)^2[h-g(h/H)]}, \quad (42)$$

where $Q = \left\{q_1 + \sum_{n=2}^{\infty}\left[\frac{Q_n}{(n-1)!}(-1)^{n-1}\right]\right\}$, Q_n $(n = 2, 3, \ldots)$ are constant expressions independent of h, $H-h$, and H. Therefore, t_y^* in Eq. (35b) is

$$t_y^* = Q\left(\frac{a}{H-h}\right)\left(\frac{h}{H-h}\right)\left(2\frac{h}{H}-\frac{h^2}{H^2}\right)\frac{1}{[h-g(h/H)]} + \frac{2a}{H}\left(1-\frac{h}{H}\right). \quad (43)$$

From the above expression, we could learn that the zero value of t_y^* is not sustained at a constant $\frac{h}{H}$ as is f_x^*.

IV. APPROXIMATE EXPRESSIONS FOR DRAG FORCE AND TORQUE

To make the present results applicable for the drag force and the torque calculation, approximate expressions of f_x^* and t_y^* are suggested in this section.

After being nondimensionalized by F_{Stokes} in Eq. (29), the drag force with respect to the nondimensional lower interval h/a and nondimensional upper interval $\frac{H-h}{a}$ is obtained through data fitting. The nondimensional drag f_x^* decreases exponentially at first and then as a power of the increasing $\frac{h}{a}$, the approximate expression is given as

$$f_x^* = k_0 + k_1 e^{-\frac{h}{2a}} + \frac{k_2}{k_3\frac{h}{a}+k_4} \quad (44)$$

and the functions $k_0 \sim k_4$ show close correlation only with $\frac{H-h}{a}$,

$$k_0 = 1 - \frac{0.37}{\frac{H-h}{a}+0.3264},$$

$$k_1 = 1.756e^{-0.68\frac{H-h}{a}} - \frac{5.906}{5.282+\frac{H-h}{a}},$$

$$k_2 = 0.6235\left(\frac{H-h}{a}\right)^2 + 6.107\frac{H-h}{a} - 2.046,$$

$$k_3 = \left(\frac{H-h}{a}\right)^2 + 1.041\frac{H-h}{a} + 1.705,$$

$$k_4 = -0.11\left(\frac{H-h}{a}\right)^2 + 2.835\frac{H-h}{a} - 2.05.$$

The above expression agrees well with the exact values in Table I and shows a mean deviation of 0.4% (Fig. 6). In most regions, it shows a very small deviation of less than 1.5%, except when the water depth is quite small, i.e., $(H-h)/a \approx 1.003$ and $h/a \le 1.003$, where the values via the fitted expression are 3.5% smaller.

By relating the nondimensional torque t_y^* with different variables composed of h and H, we find that t_y^* shows clearer correlation with $\frac{H-h}{H}$, the approximate expression being

$$t_y^* = \frac{1}{(H-h)/a}\left[q_1\left(\frac{H-h}{H}\right)^2 + q_2\frac{H-h}{H} + q_3 + \frac{q_4}{\left(1-\frac{H-h}{H}\right)^3}\right], \quad (45)$$

where the functions $q_1 \sim q_4$ could be fitted as

$$q_1 = 1 - 0.8529\left(\frac{H-h}{a}\right)^{-5.768} + \frac{2.431}{\left(\frac{H-h}{a}\right)^2+1.469},$$

$$q_2 = -\frac{0.054\,68}{\frac{H-h}{a}} - \frac{2.375}{\left(\frac{H-h}{a}\right)^{3.7}+11.83},$$

$$q_3 = -0.47\left(\frac{H-h}{a}\right)^{-1.357} + \frac{0.4849}{\left(\frac{H-h}{a}\right)^2+0.3676},$$

$$q_4 = -0.04\left(\frac{H-h}{a}\right)^{-3} + 0.04\left(\frac{H-h}{a}\right)^{-6.4}.$$

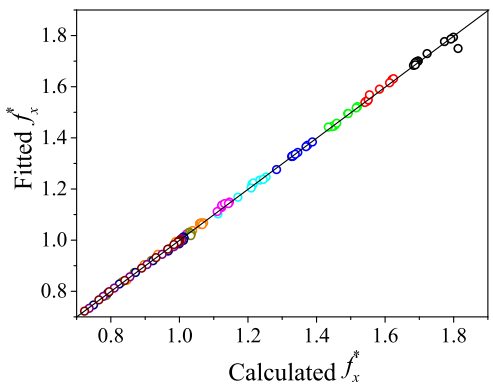

FIG. 6. Comparison of the values of f_x^* calculated by fitted expressions [Eq. (44)] (fitted) and scattered in Table III (calculated).

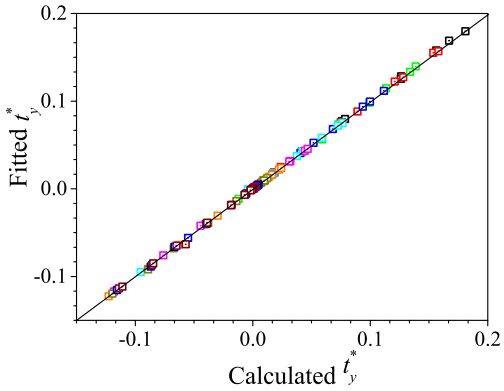

FIG. 7. Comparison of the values of t_y^* calculated by fitted expressions [Eq. (45)] (fitted) and scattered in Table IV (calculated).

This expression shows an error of less than 3% for spheres located in the lower part of the open channel ($h/H \leq 0.5$) and the near top region ($h/H > 0.8$ and $\frac{H-h}{a} \leq 5$) compared to the calculated values in Table II as shown in Fig. 7. The torque values in the other regions are quite small and negligible.

When $h/H \to 0$ and $H \to \infty$, the former expressions fitted for the drag force in Eq. (44) and torque in Eq. (45) could be simplified to a single variable function as

$$f_x^{s*} = 1 + \frac{0.6235}{\frac{h}{a} - 0.11}, \tag{46}$$

$$t_y^{s*} = 1 - \frac{0.04}{(h/a)^3}. \tag{47}$$

The function for f_x^{s*} using Eq. (46) gives a deviation of less than 1% from the data results in Table III and those of Goldman *et al.* (1967) for relative small $\frac{h}{a}$, while Eq. (47) shows a deviation of less than 2% for t_y^{s*} from the data results in Table IV and those of Goldman *et al.* (1967). The above two expressions are compared with the results $\left(f_x^{s*} = \left[1 - \frac{9}{16}\frac{a}{h} + \frac{1}{8}\left(\frac{a}{h}\right)^3\right]^{-1}\right.$ and $\left.t_y^{s*} = \left[1 + \frac{3}{16}\left(\frac{a}{h}\right)^3\right]\right)$ by Wakiya (1964), who proposed the drag and torque formula for a sphere translating along a single wall. As shown in Fig. 8, Eq. (46) agrees well with the formula by Wakiya (1964) for large $\frac{h}{a}$. According to Tables III and IV, for the condition of $h/H \leq 0.001$ (also denoted as $H/a \geq 1000$ because $h \geq a$ is always true), the above expressions are applicable.

When $(H-h)/H \to 0$ and $H \to \infty$, the former expressions fitted for the drag force in Eq. (44) and the torque in Eq. (45) could be simplified to a single variable function as

$$f_x^{s*} = 1 - \frac{0.37}{\frac{H-h}{a} + 0.3264}, \tag{48}$$

$$t_y^{s*} = -0.47\left(\frac{H-h}{a}\right)^{-2.357} + \frac{0.4849}{\left(\frac{H-h}{a}\right)^3 + 0.3676\frac{H-h}{a}} - 0.04\left(\frac{H-h}{a}\right)^{-4} + 0.04\left(\frac{H-h}{a}\right)^{-7.4}. \tag{49}$$

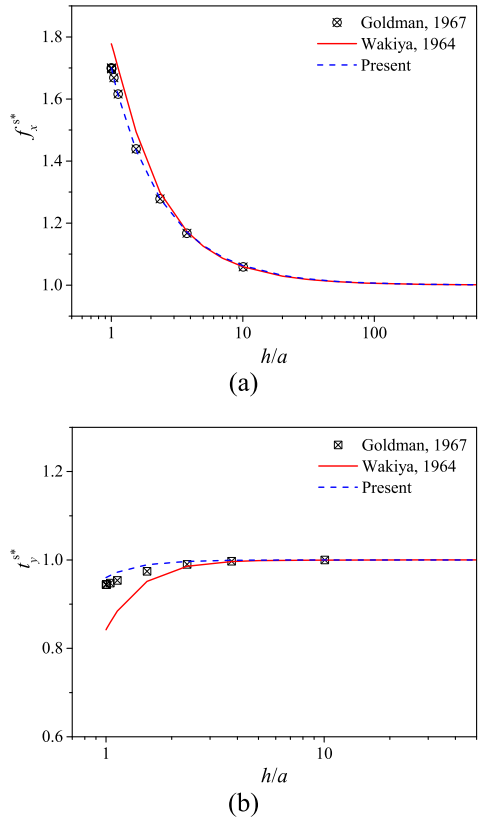

FIG. 8. Drag force and torque of a sphere near a single wall, (a) nondimensional drag and (b) nondimensional torque.

The above expression of f_x^{s*} (48) agrees well with the formula by Lauga and Squires (2005) of a sphere translating along a single slip wall and by Yang and Leal (1984) of a spherical particle moving parallel near a plane of the fluid-fluid interface in a simple shear flow (the singularity method) as shown in Fig. 9. The torque result is not compared here because the shear rate conditions in individual studies are quite different and make the comparison meaningless

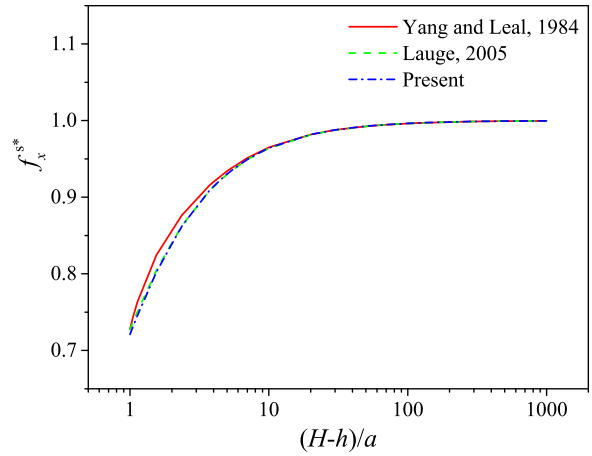

FIG. 9. Nondimensional drag of a sphere near a single free-slip wall.

$$f_x^{s*} = \begin{cases} 1 + \sum_{n=1}^{3} (-1)^n \left(\frac{3}{8}\frac{a}{H-h}\right)^n - \frac{1}{8}\left(\frac{a}{H-h}\right)^3 \\ +\frac{1}{8}\left(\frac{a}{H-h}\right)^2 \left(1 - \frac{3}{8}\frac{a}{H-h}\right) + O\left[\left(\frac{a}{H-h}\right)^4\right], \quad \text{(Yang and Leal, 1984)} \cdot \\ \left(1 + \frac{3}{8}\frac{a}{H-h}\right)^{-1}, \quad \text{(Lauga and Squires, 2005)} \end{cases} \tag{50}$$

V. CONCLUSION

In this study, a solution of a steady and uniform open channel flow under a laminar flow condition slowly passing by a stationary sphere is presented. The upper and bottom boundaries of the open channel flow are satisfied analytically, and the no slip sphere surface condition is achieved using the converged collocation technique of Ganatos *et al.* (1980). This solution is solvable for the entire valid range of h/H (the ratio of the lower interval between the sphere center and the channel bottom to the water depth) and h/a (nondimensional lower interval) even when the sphere touches the bottom wall ($h/a = 1.0$).

The nondimensional drag force f_x^* and torque t_y^* of the sphere are calculated. The values show that the drag force will be larger than that described by Stokes' drag law ($f_x^* > 1.0$) for a sphere located in the lower part of the open channel ($<0.82H$) and will be smaller ($f_x^* < 1.0$) for a sphere located in the upper part ($>0.82H$). When the sphere is located in regions near the horizontal plane of $z = 0.82H$, away from the bottom wall and away from the top surface ($H - h)/a > 10$, its drag force can be described by Stokes' drag law. The results of the nondimensional torque of the sphere show that in a steady and uniform open channel flow field, the magnitude of the torque always decreases from a maximum positive torque at the bottom to 0 and then increases in an inverse direction to obtain a maximum negative torque at the top.

For convenient application, the well-correlated approximate expressions for the nondimensional drag force and torque with respect to the corresponding length scales are proposed for a sphere of a low particle Reynolds number at any location in a uniform laminar open channel flow. The special cases of $h/H \to 0$ with $H \to \infty$ and $(H - h)/H \to 0$ with $H \to \infty$ are analysed, and the corresponding fitted expressions are consistent with the related prior research.

The results of the drag force and torque on a sphere in an open channel flow and their approximate expressions given in this investigation are based on the condition of a uniform laminar flow and a low particle Reynolds number $\mathrm{Re}_p = \frac{2u_{sc}a}{\nu} << 1$ (u_{sc} is the undisturbed upstream velocity at the height of the sphere center, and a is the sphere radius). According to the standard experimental drag-Reynolds-number relationship listed by Morsi and Alexander (1972), the Stokes drag law derived under a creeping flow condition shows a deviation of less than 2% when a particle Reynolds number is as great as 0.5, thus providing a reference range of Reynolds application for the present situation. When related to the Reynolds number of open channel flow Re_o (based on the mean velocity and hydraulic radius of open channel flow), we could find that when used in the near-bed region, the present results and expressions are applicable for almost all steady and uniform laminar open channel flows with a water depth of $H > 600a$. Here, the near bed region refers to the height of the sphere center h being less than $20a$ and the laminar open channel flow refers to a flow with $\mathrm{Re}_o < 600$ according to Chaudhry (2008). When used to the whole depth, the present results and expressions are only valid for flow with low Re_o which maintains a quite small upstream velocity u_{sc} for the sphere. For wider practical use, it is necessary to obtain the expressions applicable for moderate particle Reynolds number conditions and turbulent flow conditions.

Notably, the present solution and results are also applicable to the bacterial (Purcell, 1977; Bernardo and Moraes, 2011; and Lauga, 2016) and micro-swimmers' (Avron *et al.*, 2005 and Vladimirov, 2013) hydrodynamics (Elgeti *et al.*, 2015), whose Reynolds number is small, though the original aim of this work was to provide hydrodynamic forces for particles near the bed in open channel flow. In most applications, practical shapes are usually treated as spherical bodies, for example, sand particles and cells of micro-organisms, since this makes little difference when these shapes are quite small compared to the large flow field and are far away from another boundary. However, because actual shapes are mostly non-spherical, a spheroid approximation is usually more exact. Flow fields around a spheroid and a sphere have similar characteristics. Brenner (1964) derived the solution for the flow past a spheroid which is treated as a slightly deformed sphere. Boundaries like no-slip or free-slip walls modify the hydrodynamic stresses acting on the spheroid in the same way as acting on the sphere according to the image system (Blake and Chwang, 1974 and Lauga and Squires, 2005). However, when the body is quite close to a boundary, a spherical approximation may cause considerable error, thus a study of the spheroid under conditions similar to those in this manuscript is scheduled to be discussed in the next work.

APPENDIX A: FUNCTIONS OF THE INFINITE SERIES FORM OF u_s

$$A_n^u = \frac{1}{8(-1+2n)} r^{-n} \csc\theta \begin{Bmatrix} -\frac{2}{n}\left[-1+n-n^2+2(1+n)\cos 2\theta \cos^2\phi\right] \mathrm{P}_n^1(\cos\theta) \\ -\frac{2}{n}\left[-\left(-3+n+n^2\right)\cos 2\phi\right] \mathrm{P}_n^1(\cos\theta) \\ -4(-2+n)\cos\theta\cos^2\phi \mathrm{P}_{1+n}^1(\cos\theta) \end{Bmatrix}, \tag{A1}$$

$$B_n^u = \frac{1}{2}r^{-2-n}\Big[-(n+2\cos 2\phi + n\cos 2\phi)\csc\theta \mathrm{P}_n^1(\cos\theta) + 2n\cos^2\phi\cot\theta \mathrm{P}_{1+n}^1(\cos\theta)\Big], \tag{A2}$$

$$C_n^u = \frac{1}{2}r^{-1-n}\Big[(-n+2\cos 2\phi + n\cos 2\phi)\cot\theta \mathrm{P}_n^1(\cos\theta) + 2n\csc\theta \mathrm{P}_{1+n}^1(\cos\theta)\sin^2\phi\Big], \tag{A3}$$

$$A_n^v = \frac{r^{-n}\csc\theta\sin 2\phi}{4n(-1+2n)} \times \begin{bmatrix} \left(-3+n+n^2-\cos 2\theta - n\cos 2\theta\right)\mathrm{P}_n^1(\cos\theta) \\ +(2-n)n\cos\theta \mathrm{P}_{1+n}^1(\cos\theta) \end{bmatrix}, \tag{A4}$$

$$B_n^v = \frac{1}{2}r^{-2-n}\csc\theta\sin 2\phi\Big[-(2+n)\mathrm{P}_n^1(\cos\theta) + n\cos\theta \mathrm{P}_{1+n}^1(\cos\theta)\Big], \tag{A5}$$

$$C_n^v = \frac{1}{2}r^{-1-n}\csc\theta\sin 2\phi\Big[(2+n)\cos\theta \mathrm{P}_n^1(\cos\theta) - n\mathrm{P}_{1+n}^1(\cos\theta)\Big], \tag{A6}$$

$$A_n^w = \frac{r^{-n}}{2n(-1+2n)}\cos\phi\Big[2(1+n)\cos\theta \mathrm{P}_n^1(\cos\theta) + (-2+n)n\mathrm{P}_{1+n}^1(\cos\theta)\Big], \tag{A7}$$

$$B_n^w = -nr^{-2-n}\cos\phi \mathrm{P}_{1+n}^1(\cos\theta), \tag{A8}$$

$$C_n^w = -r^{-1-n}\cos\phi \mathrm{P}_n^1(\cos\theta). \tag{A9}$$

Here, P_n^m is the associated Legendre function of order n and degree m.

APPENDIX B: FUNCTIONS INVOLVED IN THE IMPLEMENTATION OF THE BOTTOM AND TOP BOUNDARY CONDITIONS

The double integrals involved in the implementation of the bottom and top boundary conditions

$$R_{1n} = \int_0^\infty\int_0^\infty \left(\frac{\partial}{\partial z}A_n^u(x,y,z)\Big|_{z=H-h}\right)\cos\alpha x\cos\beta y\mathrm{d}x\mathrm{d}y, \tag{B1}$$

$$S_{1n} = \int_0^\infty\int_0^\infty \left(\frac{\partial}{\partial z}B_n^u(x,y,z)\Big|_{z=H-h}\right)\cos\alpha x\cos\beta y\mathrm{d}x\mathrm{d}y, \tag{B2}$$

$$T_{1n} = \int_0^\infty\int_0^\infty \left(\frac{\partial}{\partial z}C_n^u(x,y,z)\Big|_{z=H-h}\right)\cos\alpha x\cos\beta y\mathrm{d}x\mathrm{d}y, \tag{B3}$$

$$R_{2n} = \int_0^\infty\int_0^\infty \left(\frac{\partial}{\partial z}A_n^v(x,y,z)\Big|_{z=H-h}\right)\sin\alpha x\sin\beta y\mathrm{d}x\mathrm{d}y, \tag{B4}$$

$$S_{2n} = \int_0^\infty\int_0^\infty \left(\frac{\partial}{\partial z}B_n^v(x,y,z)\Big|_{z=H-h}\right)\sin\alpha x\sin\beta y\mathrm{d}x\mathrm{d}y, \tag{B5}$$

$$T_{2n} = \int_0^\infty\int_0^\infty \left(\frac{\partial}{\partial z}C_n^v(x,y,z)\Big|_{z=H-h}\right)\sin\alpha x\sin\beta y\mathrm{d}x\mathrm{d}y, \tag{B6}$$

$$R_{3n} = \int_0^\infty\int_0^\infty \left(A_n^w(x,y,z)|_{z=H-h}\right)\sin\alpha x\cos\beta y\mathrm{d}x\mathrm{d}y, \tag{B7}$$

$$S_{3n} = \int_0^\infty\int_0^\infty \left(B_n^w(x,y,z)|_{z=H-h}\right)\sin\alpha x\cos\beta y\mathrm{d}x\mathrm{d}y, \tag{B8}$$

$$T_{3n} = \int_0^\infty\int_0^\infty \left(C_n^w(x,y,z)|_{z=H-h}\right)\sin\alpha x\cos\beta y\mathrm{d}x\mathrm{d}y, \tag{B9}$$

$$R_{4n} = \int_0^\infty\int_0^\infty \left(A_n^u(x,y,z)|_{z=-h}\right)\cos\alpha x\cos\beta y\mathrm{d}x\mathrm{d}y, \tag{B10}$$

$$S_{4n} = \int_0^\infty\int_0^\infty \left(B_n^u(x,y,z)|_{z=-h}\right)\cos\alpha x\cos\beta y\mathrm{d}x\mathrm{d}y, \tag{B11}$$

$$T_{4n} = \int_0^\infty\int_0^\infty \left(C_n^u(x,y,z)|_{z=-h}\right)\cos\alpha x\cos\beta y\mathrm{d}x\mathrm{d}y, \tag{B12}$$

$$R_{5n} = \int_0^\infty\int_0^\infty \left(A_n^v(x,y,z)|_{z=-h}\right)\sin\alpha x\sin\beta y\mathrm{d}x\mathrm{d}y, \tag{B13}$$

$$S_{5n} = \int_0^\infty\int_0^\infty \left(B_n^v(x,y,z)|_{z=-h}\right)\sin\alpha x\sin\beta y\mathrm{d}x\mathrm{d}y, \tag{B14}$$

$$T_{5n} = \int_0^\infty\int_0^\infty \left(C_n^v(x,y,z)|_{z=-h}\right)\sin\alpha x\sin\beta y\mathrm{d}x\mathrm{d}y, \tag{B15}$$

$$R_{6n} = \int_0^\infty\int_0^\infty \left(A_n^w(x,y,z)|_{z=-h}\right)\sin\alpha x\cos\beta y\mathrm{d}x\mathrm{d}y, \tag{B16}$$

$$S_{6n} = \int_0^\infty\int_0^\infty \left(B_n^w(x,y,z)|_{z=-h}\right)\sin\alpha x\cos\beta y\mathrm{d}x\mathrm{d}y, \tag{B17}$$

$$T_{6n} = \int_0^\infty\int_0^\infty \left(C_n^w(x,y,z)|_{z=-h}\right)\sin\alpha x\cos\beta y\mathrm{d}x\mathrm{d}y, \tag{B18}$$

where $A_n^i(x,y,z)$, $B_n^i(x,y,z)$, $C_n^i(x,y,z)$ $(i = u, v, w)$ represent the forms in Cartesian coordinates of A_n^i, B_n^i, C_n^i listed in Appendix A. The transformation of coordinates from spherical coordinates to Cartesian coordinates follows rules of $r = \sqrt{x^2+y^2+z^2}$, $\cos\theta = \frac{z}{\sqrt{x^2+y^2+z^2}}, (0 \le \theta \le \pi)$, and $\tan\varphi = \frac{y}{x}, (0 \le \varphi \le 2\pi)$. The primary parts in the above integrals (B1)–(B18) could be extracted as follows which are also given by Ganatos *et al.* (1980)

$$\int_0^\infty\int_0^\infty \frac{1}{(x^2+y^2+z^2)^{\frac{n+1}{2}}}\frac{\mathrm{P}_n^m\left(z/\sqrt{x^2+y^2+z^2}\right)}{(x^2+y^2)^{\frac{m}{2}}} \times \cos\alpha x\cos\beta y\mathrm{d}x\mathrm{d}y = F_1(\kappa,z,n,m), \tag{B19}$$

$$\int_0^\infty\int_0^\infty \frac{x^2}{(x^2+y^2+z^2)^{\frac{n+1}{2}}}\frac{\mathrm{P}_n^m\left(z/\sqrt{x^2+y^2+z^2}\right)}{(x^2+y^2)^{\frac{m}{2}}} \times \cos\alpha x\cos\beta y\mathrm{d}x\mathrm{d}y = F_{21}(\kappa,z,n,m) + \frac{\alpha^2}{\alpha^2+\beta^2}F_{22}(\kappa,z,n,m), \tag{B20}$$

$$\int_0^\infty\int_0^\infty \frac{xy}{(x^2+y^2+z^2)^{\frac{n+1}{2}}}\frac{\mathrm{P}_n^m\left(z/\sqrt{x^2+y^2+z^2}\right)}{(x^2+y^2)^{\frac{m}{2}}} \times \sin\alpha x\sin\beta y\mathrm{d}x\mathrm{d}y = \frac{\alpha\beta}{\alpha^2+\beta^2}F_3(\kappa,z,n,m), \tag{B21}$$

$$\int_0^\infty\int_0^\infty \frac{x}{(x^2+y^2+z^2)^{\frac{n+1}{2}}}\frac{\mathrm{P}_n^m\left(z/\sqrt{x^2+y^2+z^2}\right)}{(x^2+y^2)^{\frac{m}{2}}} \times \sin\alpha x\cos\beta y\mathrm{d}x\mathrm{d}y = \frac{\alpha}{\sqrt{\alpha^2+\beta^2}}F_4(\kappa,z,n,m), \tag{B22}$$

where

$$F_1(\kappa,z,n,m) = \frac{\pi}{2}|z|\sum_{q=0}^{\mathrm{Floor}[n/2]}\left[\sqrt{\frac{2}{\pi}}\frac{(-1)^m}{(-2)^q q!(n-2q-m)!z^{n+m}} \times (\kappa|z|)^{n-q-\frac{1}{2}}\mathrm{K}_{n-q-1/2}(\kappa|z|)\right], \tag{B23}$$

$$F_{21}(\kappa,z,n,m) = \frac{\pi}{2}|z|^3\sum_{q=0}^{\mathrm{Floor}[n/2]}\left[\sqrt{\frac{2}{\pi}}\frac{(-1)^m}{(-2)^q q!(n-2q-m)!z^{n+m}} \times (\kappa|z|)^{n-q-\frac{3}{2}}\mathrm{K}_{n-q-3/2}(\kappa|z|)\right], \tag{B24}$$

$$F_{22}(\kappa,z,n,m) = -\frac{\pi}{2}|z|^3\kappa^2 z^2 \times \sum_{q=0}^{\mathrm{Floor}[n/2]}\left[\sqrt{\frac{2}{\pi}}\frac{(-1)^m}{(-2)^q q!(n-2q-m)!z^{n+m}} \times (\kappa|z|)^{n-q-\frac{5}{2}}\mathrm{K}_{n-q-5/2}(\kappa|z|)\right], \tag{B25}$$

$$F_3(\kappa,z,n,m) = \frac{\pi}{2}\kappa^2|z|^5 \times \sum_{q=0}^{\mathrm{Floor}[n/2]}\left[\sqrt{\frac{2}{\pi}}\frac{(-1)^m}{(-2)^q q!(n-2q-m)!z^{n+m}} \times (\kappa|z|)^{n-q-\frac{5}{2}}\mathrm{K}_{n-q-5/2}(\kappa|z|)\right], \tag{B26}$$

$$F_4(\kappa,z,n,m) = \frac{\pi}{2}\kappa|z|^3 \times \sum_{q=0}^{\mathrm{Floor}[n/2]}\left[\sqrt{\frac{2}{\pi}}\frac{(-1)^m}{(-2)^q q!(n-2q-m)!z^{n+m}} \times (\kappa|z|)^{n-q-\frac{3}{2}}\mathrm{K}_{n-q-3/2}(\kappa|z|)\right]. \tag{B27}$$

Here, K_ω above is the modified Bessel function of the second kind. Function Floor[ ] gives the maximum integer which is less than or equal to the variable inside [ ]. For certain m values used in the present work, functions (B23)–(B27) can be simplified as follows:

$$F_1(\kappa,z,n,0) = \frac{\pi}{2n!}\left(\frac{|z|}{z}\right)^n \mathrm{e}^{-\kappa|z|}\kappa^{n-1}, \tag{B28}$$

$$F_{21}(\kappa,z,n,0) = \frac{-(-1+n)\pi}{2n!}\left(\frac{|z|}{z}\right)^n \mathrm{e}^{-\kappa|z|}\kappa^{-3+n} + \frac{\pi|z|}{2n!}\left(\frac{|z|}{z}\right)^n \mathrm{e}^{-\kappa|z|}\kappa^{-2+n}, \tag{B29}$$

$$F_{21}(\kappa,z,n,1) = -\frac{n\pi}{2n!}\left(\frac{|z|}{z}\right)^{n+1} \mathrm{e}^{-\kappa|z|}\kappa^{n-2}, \tag{B30}$$

$$F_{22}(\kappa,z,n,1) = -\frac{n(-2+n)\pi}{2n!}\left(\frac{|z|}{z}\right)^{n-1} \mathrm{e}^{-\kappa|z|}\kappa^{n-2} + \frac{n\pi|z|}{2n!}\left(\frac{|z|}{z}\right)^{n-1} \mathrm{e}^{-\kappa|z|}\kappa^{n-1}, \tag{B31}$$

$$F_{22}(\kappa,z,n,2) = -\frac{\pi n(-1+n)}{2n!}\left(\frac{|z|}{z}\right)^n \mathrm{e}^{-\kappa|z|}\kappa^{n-1}, \tag{B32}$$

$$F_{22}(\kappa,z,n,0) = \mathrm{e}^{-\kappa|z|}\kappa^{n-3}\left(\frac{|z|}{z}\right)^n\left[-\frac{\pi(-1+n)(-3+n)}{2n!} + \frac{\pi(-3+2n)|z|}{2n!}\kappa - \frac{\pi z^2}{2n!}\kappa^2\right], \tag{B33}$$

$$F_3(\kappa,z,n,2) = \frac{\pi n(-1+n)}{2n!}\left(\frac{|z|}{z}\right)^n \mathrm{e}^{-\kappa|z|}\kappa^{n-1}, \tag{B34}$$

$$F_3(\kappa,z,n,1) = \frac{\pi n(-2+n)}{2n!}\left(\frac{|z|}{z}\right)^{n+1} \mathrm{e}^{-\kappa|z|}\kappa^{n-2} - \frac{\pi n|z|}{2n!}\left(\frac{|z|}{z}\right)^{n+1} \mathrm{e}^{-\kappa|z|}\kappa^{n-1}, \tag{B35}$$

$$F_4(\kappa,z,n,1) = -\frac{\pi n}{2n!}\left(\frac{|z|}{z}\right)^{n+1} \mathrm{e}^{-\kappa|z|}\kappa^{n-1}. \tag{B36}$$

By substituting (A1)–(A9) and (B19)–(B22), functions R_{in}, S_{in}, T_{in} $(i = 1, 2, 3, 4, 5, 6)$ in (B1)–(B18) are obtained as

$$R_{1n} = \frac{1}{4n(-1+2n)}\begin{bmatrix} (-2+n)n(1+n)^2F_1(\kappa, H-h, n, 0) \\ +6\cos 2\gamma F_{22}(\kappa, H-h, n, 2) \\ -n(1+n)(-2+n)(1+2n)z_2F_1(\kappa, H-h, 1+n, 0) \\ -4n(1+n)F_{21}(\kappa, H-h, 1+n, 1) \\ -n(1+n)\cos 2\gamma F_{22}(\kappa, H-h, n, 2) \\ -4n(1+n)\cos^2\gamma F_{22}(\kappa, H-h, 1+n, 1) \\ +(-2+n)(1+2n)(H-h)\cos 2\gamma F_{22}(\kappa, H-h, 1+n, 2) \end{bmatrix}, \tag{B37}$$

$$S_{1n} = \frac{1}{2}\left[n(1+n)(2+n)F_1(\kappa, H-h, 2+n, 0) - n\cos 2\gamma F_{22}(\kappa, H-h, 2+n, 2)\right], \tag{B38}$$

$$T_{1n} = \frac{1}{2}\left[n(1+n)^2F_1(\kappa, H-h, 1+n, 0) + (-1+n)\cos 2\gamma F_{22}(\kappa, H-h, 1+n, 2)\right], \tag{B39}$$

$$R_{2n} = -\frac{\cos\gamma\sin\gamma}{2n(-1+2n)}\begin{bmatrix} \left(-6+n+n^2\right)F_3(\kappa, H-h, n, 2) \\ +2n(1+n)F_3(\kappa, H-h, 1+n, 1) \\ +\left(2+3n-2n^2\right)(H-h)F_3(\kappa, H-h, 1+n, 2) \end{bmatrix}, \tag{B40}$$

$$S_{2n} = -n\cos\gamma\sin\gamma F_3(\kappa, H-h, 2+n, 2), \tag{B41}$$

$$T_{2n} = (-1+n)\cos\gamma\sin\gamma F_3(\kappa, H-h, 1+n, 2), \tag{B42}$$

$$R_{3n} = \frac{1}{2}\cos\gamma\left[\frac{\left(2+n-n^2\right)F_4(\kappa, H-h, -1+n, 1)}{n(-1+2n)} + z_2F_4(\kappa, H-h, n, 1)\right], \tag{B43}$$

$$S_{3n} = -n\cos\gamma F_4(\kappa, H-h, 1+n, 1), \tag{B44}$$

$$T_{3n} = -\cos\gamma F_4(\kappa, H-h, n, 1), \tag{B45}$$

$$R_{4n} = \frac{1}{4n(n-1)(2n-1)}\left\{\begin{array}{l} (1-n)(-2+n)n^2F_1(\kappa, -h, -1+n, 0) \\ +(-1+n)(-2+n)n(1+2n)(-h)F1(\kappa, -h, n, 0) \\ +2\left(-1+n^2\right)[2F_{21}(\kappa, -h, n, 1) + F_{22}(\kappa, -h, n, 1)] \\ +\cos 2\gamma\begin{bmatrix} \left(-4+n^2\right)F_{22}(\kappa, -h, -1+n, 2) \\ +2\left(-1+n^2\right)F_{22}(\kappa, -h, n, 1) \\ +\left(2+3n-2n^2\right)(-h)F_{22}(\kappa, -h, n, 2) \end{bmatrix} \end{array}\right\}, \tag{B46}$$

$$S_{4n} = \frac{1}{2}[-n(1+n)F_1(\kappa, -h, 1+n, 0) + \cos 2\gamma F_{22}(\kappa, -h, 1+n, 2)], \tag{B47}$$

$$T_{4n} = \frac{1}{2}\left[-n(1+n)F_1(\kappa, -h, n, 0) - \cos 2\gamma F_{22}(\kappa, -h, n, 2)\right], \tag{B48}$$

$$R_{5n} = \frac{1}{2(-1+n)n(-1+2n)}\cos\gamma\sin\gamma \times\begin{bmatrix} \left(-4+n^2\right)F_3(\kappa, -h, -1+n, 2) \\ +2\left(-1+n^2\right)F_3(\kappa, -h, n, 1) \\ +\left(2+3n-2n^2\right)(-h)F_3(\kappa, -h, n, 2) \end{bmatrix}, \tag{B49}$$

$$S_{5n} = \cos\gamma\sin\gamma F_3(\kappa, -h, 1+n, 2), \tag{B50}$$

$$T_{5n} = -\cos\gamma\sin\gamma F_3(\kappa, -h, n, 2), \tag{B51}$$

$$R_{6n} = \frac{1}{2}\cos\gamma\left[\frac{2+n-n^2}{n(-1+2n)}F_4(\kappa, -h, -1+n, 1) - hF_4(\kappa, -h, n, 1)\right], \tag{B52}$$

$$S_{6n} = -n\cos\gamma F_4(\kappa, -h, 1+n, 1), \tag{B53}$$

$$T_{6n} = -\cos\gamma F_4(\kappa, -h, n, 1). \tag{B54}$$

APPENDIX C: INTEGRAND FUNCTIONS OF THE DOUBLE INTEGRAL FORMS OF u_b

After the bottom and top boundary conditions were satisfied, $\boldsymbol{u}_b$ is transformed to the infinite series form from the original double integral form. The integrands of these double integrals are as follows:

$$\Lambda_n^{11} = G_3R_{3n}\cos\gamma + G_6R_{6n}\cos\gamma + R_{1n}\left(G_{12} + G_{11}\cos^2\gamma\right) + R_{4n}\left(G_{42} + G_{41}\cos^2\gamma\right) + G_2R_{2n}\cos\gamma\sin\gamma + G_5R_{5n}\cos\gamma\sin\gamma, \tag{C1}$$

$$\Lambda_n^{12} = G_3S_{3n}\cos\gamma + G_6S_{6n}\cos\gamma + S_{1n}\left(G_{12} + G_{11}\cos^2\gamma\right) + S_{4n}\left(G_{42} + G_{41}\cos^2\gamma\right) + G_2S_{2n}\cos\gamma\sin\gamma + G_5S_{5n}\cos\gamma\sin\gamma, \tag{C2}$$

$$\Lambda_n^{13} = G_3T_{3n}\cos\gamma + G_6T_{6n}\cos\gamma + T_{1n}\left(G_{12} + G_{11}\cos^2\gamma\right) + T_{4n}\left(G_{42} + G_{41}\cos^2\gamma\right) + G_2T_{2n}\cos\gamma\sin\gamma + G_5T_{5n}\cos\gamma\sin\gamma, \tag{C3}$$

$$\Lambda_n^{21} = R_{2n}\left(H_{22} + H_{21}\cos^2\gamma\right) + R_{5n}\left(H_{52} + H_{51}\cos^2\gamma\right) + H_3R_{3n}\sin\gamma + H_6R_{6n}\sin\gamma + H_1R_{1n}\cos\gamma\sin\gamma + H_4R_{4n}\cos\gamma\sin\gamma, \tag{C4}$$

$$\Lambda_n^{22} = S_{2n}\left(H_{22} + H_{21}\cos^2\gamma\right) + S_{5n}\left(H_{52} + H_{51}\cos^2\gamma\right) + H_3S_{3n}\sin\gamma + H_6S_{6n}\sin\gamma + H_1S_{1n}\cos\gamma\sin\gamma + H_4S_{4n}\cos\gamma\sin\gamma, \tag{C5}$$

$$\Lambda_n^{23} = T_{2n}\left(H_{22} + H_{21}\cos^2\gamma\right) + T_{5n}\left(H_{52} + H_{51}\cos^2\gamma\right) + H_3T_{3n}\sin\gamma + H_6T_{6n}\sin\gamma + H_1T_{1n}\cos\gamma\sin\gamma + H_4T_{4n}\cos\gamma\sin\gamma, \tag{C6}$$

$$\Lambda_n^{31} = I_3R_{3n} + I_6R_{6n} + I_1R_{1n}\cos\gamma + I_4R_{4n}\cos\gamma + I_2R_{2n}\sin\gamma + I_5R_{5n}\sin\gamma, \tag{C7}$$

$$\Lambda_n^{32} = I_3S_{3n} + I_6S_{6n} + I_1S_{1n}\cos\gamma + I_4S_{4n}\cos\gamma + I_2S_{2n}\sin\gamma + I_5S_{5n}\sin\gamma, \tag{C8}$$

$$\Lambda_n^{33} = I_3T_{3n} + I_6T_{6n} + I_1T_{1n}\cos\gamma + I_4T_{4n}\cos\gamma + I_2T_{2n}\sin\gamma + I_5T_{5n}\sin\gamma, \tag{C9}$$

where functions R_{in}, S_{in}, T_{in} (i = 1, 2, 3, 4, 5, 6) are given in (B37)–(B54) in Appendix B, functions G_{11}–I_6 in (C1)–(C9) are as follows, σ and τ below represent κH and $\kappa(z+h)$, respectively,

$$G_{11} = \frac{-2\tau\frac{\sinh\sigma}{\cosh\tau} + \tau\cosh\tau(\sigma\cosh\sigma + \sinh\sigma) + \sinh\tau[\sinh\sigma - \sigma(\cosh\sigma + \tau\sinh\sigma)]}{\kappa[2\tau - \sinh(\tau)]}, \tag{C10}$$

$$G_{12} = \frac{\sinh\sigma}{\kappa\cosh\tau}, \tag{C11}$$

$$G_2 = \frac{2\tau\frac{\sinh\sigma}{\cosh\tau} - \tau\cosh\tau(\sigma\cosh\sigma + \sinh\sigma) + \sinh\tau[\sigma\cosh\sigma + (-1+\tau\sigma)\sinh\sigma]}{\kappa[2\tau - \sinh(2\tau)]}, \tag{C12}$$

$$G_3 = -\frac{\cosh\tau[\tau\sigma\cosh\sigma + (\tau - 2\sigma)\sinh\sigma] + \sinh\tau(\sigma\cosh\sigma + \sinh\sigma - \tau\sigma\sinh\sigma)}{2\tau - \sinh(2\tau)}, \tag{C13}$$

$$G_{41} = -\frac{2[\sigma\cosh\tau\sinh(\tau-\sigma) + \tau\sinh\sigma]\tanh\tau}{-2\tau + \sinh(2\tau)}, \tag{C14}$$

$$G_{42} = \cosh\sigma - \sinh\sigma\tanh\tau, \tag{C15}$$

$$G_5 = \frac{2[\sigma\cosh\tau\sinh(\tau-\sigma) + \tau\sinh\sigma]\tanh\tau}{-2\tau + \sinh(2\tau)}, \tag{C16}$$

$$G_6 = \frac{2[\sigma\cosh\tau\sinh(\tau-\sigma) + \tau\sinh\sigma]}{2\tau - \sinh(2\tau)}, \tag{C17}$$

$$H_1 = \frac{2\tau\frac{\sinh\sigma}{\cosh\tau} - \tau\cosh\tau(\sigma\cosh\sigma + \sinh\sigma) + \sinh\tau[\sigma\cosh\sigma + (-1+\tau\sigma)\sinh\sigma]}{\kappa[2\tau - \sinh(2\tau)]}, \tag{C18}$$

$$H_{21} = \frac{2\tau\frac{\sinh\sigma}{\cosh\tau} - \tau\cosh\tau(\sigma\cosh\sigma + \sinh\sigma) + \sinh\tau[\sigma\cosh\sigma + (-1+\tau\sigma)\sinh\sigma]}{\kappa[2\tau - \sinh(2\tau)]}, \tag{C19}$$

$$H_{22} = \frac{\tau\cosh\tau(\sigma\cosh\sigma + \sinh\sigma) - (\sigma\cosh\sigma + \sinh\sigma + \sigma\tau\sinh\sigma)\sinh\tau}{2\kappa(\tau - \cosh\tau\sinh\tau)}, \tag{C20}$$

$$H_3 = \frac{\cosh\tau(\tau\sigma\cosh\sigma + (\tau-2\sigma)\sinh\sigma) + \sinh\tau(\sigma\cosh\sigma + \sinh\sigma - \tau\sigma\sinh\sigma)}{2\tau - \sinh(2\tau)}, \tag{C21}$$

$$H_4 = \frac{2[\sigma\cosh\tau\sinh(\tau-\sigma) + \tau\sinh\sigma]\tanh\tau}{-2\tau + \sinh(2\tau)}, \tag{C22}$$

$$H_{51} = \frac{2[\sigma\cosh\tau\sinh(\tau-\sigma) + \tau\sinh\sigma]\tanh\tau}{-2\tau + \sinh(2\tau)}, \tag{C23}$$

$$H_{52} = \frac{-\sigma\cosh(2\tau-\sigma) + (-2\tau+\sigma)\cosh\sigma + \sinh(2\tau-\sigma) + \sinh\sigma}{-2\tau + \sinh(2\tau)}, \tag{C24}$$

$$H_6 = \frac{2[\sigma\cosh\tau\sinh(\tau-\sigma) + \tau\sinh\sigma]}{-2\tau + \sinh(2\tau)}, \tag{C25}$$

$$I_1 = \frac{-\tau\sigma\cosh\sigma\sinh\tau + [\tau\sigma\cosh\tau + (\tau-\sigma)\sinh\tau]\sinh\sigma}{\kappa[2\tau - \sinh(2\tau)]}, \tag{C26}$$

$$I_2 = \frac{\tau\sigma\cosh\sigma\sinh\tau - [\tau\sigma\cosh\tau + (\tau-\sigma)\sinh\tau]\sinh\sigma}{\kappa(2\tau - \sinh 2\tau)}, \tag{C27}$$

$$I_3 = \frac{\sinh\tau[\tau\sigma\cosh\sigma - (\tau+\sigma)\sinh\sigma] - \cosh\tau[-2\sigma\cosh\sigma + (2+\tau\sigma)\sinh\sigma]}{2\tau - \sinh(2\tau)}, \tag{C28}$$

$$I_4 = \frac{\sigma\sinh(2\tau-\sigma) + (-2\tau+\sigma)\sinh\sigma}{-2\tau + \sinh(2\tau)}, \tag{C29}$$

$$I_5 = -\frac{\sigma\sinh(2\tau-\sigma) + (-2\tau+\sigma)\sinh\sigma}{-2\tau + \sinh(2\tau)}, \tag{C30}$$

$$I_6 = \frac{\sigma\cosh(2\tau-\sigma) + (-2\tau+\sigma)\cosh\sigma + 2\cosh\tau\sinh(\tau-\sigma)}{-2\tau + \sinh(2\tau)}. \tag{C31}$$

APPENDIX D: INTEGRAND FUNCTIONS OF THE SINGLE INTEGRAL FORMS OF u_b

The functions used in solving the inner integrals of $\boldsymbol{u}_b$ and the integrands after solving the inner integrals are formulated as

$$O_1 = \int_0^{\pi/2} \cos(\kappa x\cos\gamma)\cos(\kappa y\sin\gamma)\mathrm{d}\gamma = \frac{\pi}{2}\mathrm{J}_0\left(\kappa\sqrt{x^2+y^2}\right), \tag{D1}$$

$$O_2 = \int_0^{\pi/2} \cos^2\gamma\cos(\kappa x\cos\gamma)\cos(\kappa y\sin\gamma)\mathrm{d}\gamma = \frac{\pi x^2\mathrm{J}_0\left(\kappa\sqrt{x^2+y^2}\right)}{2(x^2+y^2)} + \frac{\pi\left(y^2-x^2\right)\mathrm{J}_1\left(\kappa\sqrt{x^2+y^2}\right)}{2(x^2+y^2)^{3/2}\kappa}, \tag{D2}$$

$$O_3 = \int_0^{\frac{1}{2}\pi} \cos^4\theta\cos(\kappa x\cos\theta)\cos(\kappa y\sin\theta)\mathrm{d}\theta = \frac{\pi\left[-3\left(x^4-6x^2y^2+y^4\right)+x^4\left(x^2+y^2\right)\kappa^2\right]\mathrm{J}_0\left(\kappa\sqrt{x^2+y^2}\right)}{2(x^2+y^2)^3\kappa^2} + \frac{\pi\left[3\left(x^4-6x^2y^2+y^4\right)-x^2\left(x^2-3y^2\right)\left(x^2+y^2\right)\kappa^2\right]\mathrm{J}_1\left(\kappa\sqrt{x^2+y^2}\right)}{(x^2+y^2)^{7/2}\kappa^3}, \tag{D3}$$

$$O_4 = \int_0^{\frac{1}{2}\pi} \cos\theta\sin\theta\sin(\kappa x\cos\theta)\sin(\kappa y\sin\theta)\mathrm{d}\theta = -\frac{\pi xy\mathrm{J}_0\left(\kappa\sqrt{x^2+y^2}\right)}{2(x^2+y^2)} + \frac{\pi xy\mathrm{J}_1\left(\kappa\sqrt{x^2+y^2}\right)}{(x^2+y^2)^{3/2}\kappa}, \tag{D4}$$

$$O_5 = \int_0^{\frac{1}{2}\pi} \cos^2\theta \cos\theta \sin\theta \sin(\kappa x \cos\theta) \sin(\kappa y \sin\theta) \mathrm{d}\theta = \frac{\pi x y \left[12(x-y)(x+y) - x^2\left(x^2+y^2\right)\kappa^2\right] \mathrm{J}_0\left(\kappa\sqrt{x^2+y^2}\right)}{2\left(x^2+y^2\right)^3 \kappa^2}$$
$$+ \frac{\pi y \left[-24x(x-y)(x+y) + x\left(5x^2-3y^2\right)\left(x^2+y^2\right)\kappa^2\right] \mathrm{J}_1\left(\kappa\sqrt{x^2+y^2}\right)}{2\left(x^2+y^2\right)^{7/2}\kappa^3}, \tag{D5}$$

$$O_6 = \int_0^{\frac{1}{2}\pi} \cos\theta \sin(\kappa x \cos\theta) \cos(\kappa y \sin\theta) \mathrm{d}\theta = \frac{\pi x \mathrm{J}_1\left(\kappa\sqrt{x^2+y^2}\right)}{2\sqrt{x^2+y^2}}, \tag{D6}$$

$$O_7 = \int_0^{\frac{1}{2}\pi} \cos^2\theta \cos\theta \sin(\kappa x \cos\theta) \cos(\kappa y \sin\theta) \mathrm{d}\theta$$
$$= \frac{\pi\left(x^3 - 3xy^2\right) \mathrm{J}_0\left(\kappa\sqrt{x^2+y^2}\right)}{2\left(x^2+y^2\right)^2\kappa} + \frac{\pi x\left[6y^2 + x^2\left(-2 + \left(x^2+y^2\right)\kappa^2\right)\right] \mathrm{J}_1\left(\kappa\sqrt{x^2+y^2}\right)}{2\left(x^2+y^2\right)^{5/2}\kappa^2}. \tag{D7}$$

Here, $\mathrm{J}_0\left(\kappa\sqrt{x^2+y^2}\right)$ and $\mathrm{J}_1\left(\kappa\sqrt{x^2+y^2}\right)$ represent Bessel functions of the first kind of order 0 and order 1, respectively,

$$\zeta_n^{11} = O_1 \left\{ \begin{array}{l} G_{12}\left[\begin{array}{l} \frac{(-2+n)(1+n)^2 F_1(\kappa, H-h, n, 0)}{4(-1+2n)} + \frac{(2-n)(1+n)(1+2n)(H-h)F_1(\kappa, H-h, 1+n, 0)}{4(-1+2n)} + \frac{(-1-n)F_{21}(\kappa, H-h, 1+n, 1)}{-1+2n} \\ -\frac{3F_{22}(\kappa, H-h, n, 2)}{2n(-1+2n)} + \frac{(1+n)F_{22}(\kappa, H-h, n, 2)}{4(-1+2n)} + \frac{(2-n)(1+2n)(H-h)F_{22}(\kappa, H-h, 1+n, 2)}{4n(-1+2n)} \end{array} \right] \\ +G_{42}\left[\begin{array}{l} \frac{(2-n)n(nF_1(\kappa, -h, -1+n, 0) - (1+2n)(-h)F_1(\kappa, -h, n, 0)) + 4(1+n)F_{21}(\kappa, -h, n, 1)}{4n(-1+2n)} \\ -\frac{\left(-4+n^2\right)F_{22}(\kappa, -h, -1+n, 2)}{4(-1+n)n(-1+2n)} - \frac{(2+(3-2n)n)(-h)F_{22}(\kappa, -h, n, 2)}{4(-1+n)n(-1+2n)} \end{array} \right] \end{array} \right\}$$
$$+ O_3 \left\{ \begin{array}{l} G_{11}\left[\frac{(-1-n)F_{22}(\kappa, H-h, n, 2)}{2(-1+2n)} + \frac{3F_{22}(\kappa, H-h, n, 2)}{n(-1+2n)} + \frac{(-1-n)F_{22}(\kappa, H-h, 1+n, 1)}{-1+2n} + \frac{(-2+n)(1+2n)(H-h)F_{22}(\kappa, H-h, 1+n, 2)}{2n(-1+2n)}\right] \\ +\frac{1}{2n(-1+2n)} G_2\left[\left(-6+n+n^2\right)F_3(\kappa, H-h, n, 2) + 2n(1+n)F_3(\kappa, H-h, 1+n, 1) + (2+(3-2n)n)z2F_3(\kappa, H-h, 1+n, 2)\right] \\ +\frac{1}{2(-1+n)n(-1+2n)} G_{41}\left[\left(-4+n^2\right)F_{22}(\kappa, -h, -1+n, 2) + 2\left(-1+n^2\right)F_{22}(\kappa, -h, n, 1) + (2+(3-2n)n)(-h)F_{22}(\kappa, -h, n, 2)\right] \\ -\frac{G_5\left[\left(-4+n^2\right)F_3(\kappa, -h, -1+n, 2) + 2\left(-1+n^2\right)F_3(\kappa, -h, n, 1) + (2+(3-2n)n)(-h)F_3(\kappa, -h, n, 2)\right]}{2(-1+n)n(-1+2n)} \end{array} \right\}$$
$$+ O_2 \left\{ \begin{array}{l} G_{11}\left[\begin{array}{l} \frac{(-2+n)(1+n)^2 F_1(\kappa, H-h, n, 0)}{4(-1+2n)} + \frac{(2-n)(1+n)(1+2n)(H-h)F_1(\kappa, H-h, 1+n, 0)}{4(-1+2n)} \\ +\frac{(-1-n)F_{21}(\kappa, H-h, 1+n, 1)}{-1+2n} - \frac{3F_{22}(\kappa, H-h, n, 2)}{2n(-1+2n)} + \frac{(1+n)F_{22}(\kappa, H-h, n, 2)}{4(-1+2n)} + \frac{(2-n)(1+2n)(H-h)F_{22}(\kappa, H-h, 1+n, 2)}{4n(-1+2n)} \end{array} \right] \\ +G_{12}\left[\frac{(-1-n)F_{22}(\kappa, H-h, n, 2)}{2(-1+2n)} + \frac{3F_{22}(\kappa, H-h, n, 2)}{n(-1+2n)} + \frac{(-1-n)F_{22}(\kappa, H-h, 1+n, 1)}{-1+2n} + \frac{(-2+n)(1+2n)(H-h)F_{22}(\kappa, H-h, 1+n, 2)}{2n(-1+2n)}\right] \end{array} \right\}$$
$$+ O_2 \left\{ \begin{array}{l} -\frac{1}{2n(-1+2n)} G_2\left[\left(-6+n+n^2\right)F_3(\kappa, H-h, n, 2) + 2n(1+n)F_3(\kappa, H-h, 1+n, 1) + (2+(3-2n)n)(H-h)F_3(\kappa, H-h, 1+n, 2)\right] \\ +\frac{1}{2(-1+n)n(-1+2n)} G_{42}\left[\left(-4+n^2\right)F_{22}(\kappa, -h, -1+n, 2) + 2\left(-1+n^2\right)F_{22}(\kappa, -h, n, 1) + (2+(3-2n)n)(-h)F_{22}(\kappa, -h, n, 2)\right] \\ +G_{41}\left[\begin{array}{l} \frac{(2-n)n(nF_1(\kappa, -h, -1+n, 0) - (1+2n)(-h)F_1(\kappa, -h, n, 0)) + 4(1+n)F_{21}(\kappa, -h, n, 1)}{4n(-1+2n)} \\ -\frac{\left(-4+n^2\right)F_{22}(\kappa, -h, -1+n, 2)}{4(-1+n)n(-1+2n)} - \frac{(2+(3-2n)n)(-h)F_{22}(\kappa, -h, n, 2)}{4(-1+n)n(-1+2n)} \end{array} \right] \\ +\frac{G_5\left[\left(-4+n^2\right)F_3(\kappa, -h, -1+n, 2) + 2\left(-1+n^2\right)F_3(\kappa, -h, n, 1) + (2+(3-2n)n)(-h)F_3(\kappa, -h, n, 2)\right]}{2(-1+n)n(-1+2n)} \\ +\frac{1}{2}G_6\left[\frac{\left(2+n-n^2\right)F_4(\kappa, -h, -1+n, 1)}{n(-1+2n)} + (-h)F_4(\kappa, -h, n, 1)\right] + \frac{1}{2}G_3\left[\frac{\left(2+n-n^2\right)F_4(\kappa, H-h, -1+n, 1)}{n(-1+2n)} + (H-h)F_4(\kappa, H-h, n, 1)\right] \end{array} \right\}, \tag{D8}$$

$$\zeta_n^{12} = O_1\left\{ G_{12}\left[\frac{1}{2}n(1+n)(2+n)F_1(\kappa,H-h,2+n,0)+\frac{1}{2}nF_{22}(\kappa,H-h,2+n,2)\right]+G_{42}\left[-\frac{1}{2}n(1+n)F_1(\kappa,-h,1+n,0)-\frac{1}{2}F_{22}(\kappa,-h,1+n,2)\right]\right\}$$
$$+O_3\left\{-G_{11}nF_{22}(\kappa,H-h,2+n,2)+G_2nF_3(\kappa,H-h,2+n,2)+G_{41}F_{22}(\kappa,-h,1+n,2)-G_5F_3(\kappa,-h,1+n,2)\right\}$$
$$+O_2\left\{\begin{array}{l}+G_{11}\left[\frac{1}{2}n(1+n)(2+n)F_1(\kappa,H-h,2+n,0)+\frac{1}{2}nF_{22}(\kappa,H-h,2+n,2)\right]-G_{12}nF_{22}(\kappa,H-h,2+n,2)\\ -G_2nF_3(\kappa,H-h,2+n,2)-G_3nF_4(\kappa,H-h,1+n,1)\\ +G_{41}\left[-\frac{1}{2}n(1+n)F_1(\kappa,-h,1+n,0)-\frac{1}{2}F_{22}(\kappa,-h,1+n,2)\right]+G_{42}F_{22}(\kappa,-h,1+n,2)+G_5F_3(\kappa,-h,1+n,2)-G_6nF_4(\kappa,-h,1+n,1)\end{array}\right\},$$

(D9)

$$\zeta_n^{13} = O_1\left\{ G_{12}\left[\frac{1}{2}n(1+n)^2F_1(\kappa,H-h,1+n,0)+\frac{1}{2}(1-n)F_{22}(\kappa,H-h,1+n,2)\right]+G_{42}\left[-\frac{1}{2}n(1+n)F_1(\kappa,-h,n,0)+\frac{1}{2}F_{22}(\kappa,-h,n,2)\right]\right\}$$
$$+O_3\left\{ G_{11}(-1+n)F_{22}(\kappa,H-h,1+n,2)+G_2(1-n)F_3(\kappa,H-h,1+n,2)-G_{41}F_{22}(\kappa,-h,n,2)+G_5F_3(\kappa,-h,n,2)\right\}$$
$$+O_2\left\{\begin{array}{l}G_{11}\left[\frac{1}{2}n(1+n)^2F_1(\kappa,H-h,1+n,0)+\frac{1}{2}(1-n)F_{22}(\kappa,H-h,1+n,2)\right]+G_{12}(-1+n)F_{22}(\kappa,H-h,1+n,2)+G_2(-1+n)F_3(\kappa,H-h,1+n,2)\\ -G_3F_4(\kappa,H-h,n,1)+G_{41}\left[-\frac{1}{2}n(1+n)F_1(\kappa,-h,n,0)+\frac{1}{2}F_{22}(\kappa,-h,n,2)\right]-G_{42}F_{22}(\kappa,-h,n,2)-G_5F_3(\kappa,-h,n,2)-G_6F_4(\kappa,-h,n,1)\end{array}\right\},$$

(D10)

$$\zeta_n^{21} = O_5\left\{\begin{array}{l}H_1\left[\frac{(-1-n)F_{22}(\kappa,H-h,1+n,1)}{-1+2n}+2\left(\frac{(-1-n)F_{22}(\kappa,H-h,n,2)}{4(-1+2n)}+\frac{3F_{22}(\kappa,H-h,n,2)}{2n(-1+2n)}+\frac{(-2+n)(1+2n)(H-h)F_{22}(\kappa,H-h,1+n,2)}{4n(-1+2n)}\right)\right]\\ -\frac{1}{2n(-1+2n)}H_{21}\left[\left(-6+n+n^2\right)F_3(\kappa,H-h,n,2)+2n(1+n)F_3(\kappa,H-h,1+n,1)+(2+(3-2n)n)(H-h)F_3(\kappa,H-h,1+n,2)\right]\\ +\frac{1}{2(-1+n)n(-1+2n)}H_4\left[\left(-4+n^2\right)F_{22}(\kappa,-h,-1+n,2)+2\left(-1+n^2\right)F_{22}(\kappa,-h,n,1)+(2+(3-2n)n)(-h)F_{22}(\kappa,-h,n,2)\right]\\ +\frac{H_{51}\left[\left(-4+n^2\right)F_3(\kappa,-h,-1+n,2)+2\left(-1+n^2\right)F_3(\kappa,-h,n,1)+(2+(3-2n)n)(-h)F_3(\kappa,-h,n,2)\right]}{2(-1+n)n(-1+2n)}\end{array}\right\}$$
$$+O_4\left\{\begin{array}{l}H_1\left[\begin{array}{l}\frac{(-2+n)(1+n)^2F_1(\kappa,H-h,n,0)}{4(-1+2n)}+\frac{(2-n)(1+n)(1+2n)(H-h)F_1(\kappa,H-h,1+n,0)}{4(-1+2n)}+\frac{(-1-n)F_{21}(\kappa,H-h,1+n,1)}{-1+2n}\\ -\frac{3F_{22}(\kappa,H-h,n,2)}{2n(-1+2n)}+\frac{(1+n)F_{22}(\kappa,H-h,n,2)}{4(-1+2n)}+\frac{(2-n)(1+2n)(H-h)F_{22}(\kappa,H-h,1+n,2)}{4n(-1+2n)}\end{array}\right]\\ -\frac{1}{2n(-1+2n)}H_{22}\left[\left(-6+n+n^2\right)F_3(\kappa,H-h,n,2)+2n(1+n)F_3(\kappa,H-h,1+n,1)+(2+(3-2n)n)(H-h)F_3(\kappa,H-h,1+n,2)\right]\\ +\frac{1}{2}H_3\left[\frac{\left(2+n-n^2\right)F_4(\kappa,H-h,-1+n,1)}{n(-1+2n)}+(H-h)F_4(\kappa,H-h,n,1)\right]\\ +H_4\left[\begin{array}{l}\frac{(2-n)n(nF_1(\kappa,-h,-1+n,0)-(1+2n)(-h)F_1(\kappa,-h,n,0))+4(1+n)F_{21}(\kappa,-h,n,1)}{4n(-1+2n)}+\frac{\left(-1+n^2\right)F_{22}(\kappa,-h,n,1)}{2(-1+n)n(-1+2n)}\\ -\frac{\left(-4+n^2\right)F_{22}(\kappa,-h,-1+n,2)+2\left(-1+n^2\right)F_{22}(\kappa,-h,n,1)+(2+(3-2n)n)(-h)F_{22}(\kappa,-h,n,2)}{4(-1+n)n(-1+2n)}\end{array}\right]\\ +\frac{H_{52}\left[\left(-4+n^2\right)F_3(\kappa,-h,-1+n,2)+2\left(-1+n^2\right)F_3(\kappa,-h,n,1)+(2+(3-2n)n)(-h)F_3(\kappa,-h,n,2)\right]}{2(-1+n)n(-1+2n)}\\ +\frac{1}{2}H_6\left[\frac{\left(2+n-n^2\right)F_4(\kappa,-h,-1+n,1)}{n(-1+2n)}+(-h)F_4(\kappa,-h,n,1)\right]\end{array}\right\},$$

(D11)

$$\zeta_n^{22} = O_5\left\{-H_1nF_{22}(\kappa,H-h,2+n,2)-H_{21}nF_3(\kappa,H-h,2+n,2)+H_4F_{22}(\kappa,-h,1+n,2)+H_{51}F_3(\kappa,-h,1+n,2)\right\}$$
$$+O_4\left\{\begin{array}{l}H_1\left[\frac{1}{2}n(1+n)(2+n)F_1(\kappa,H-h,2+n,0)+\frac{1}{2}nF_{22}(\kappa,H-h,2+n,2)\right]-H_{22}nF_3(\kappa,H-h,2+n,2)-H_3nF_4(\kappa,H-h,1+n,1)\\ +H_4\left[-\frac{1}{2}n(1+n)F_1(\kappa,-h,1+n,0)-\frac{1}{2}F_{22}(\kappa,-h,1+n,2)\right]+H_{52}F_3(\kappa,-h,1+n,2)-H_6nF_4(\kappa,-h,1+n,1)\end{array}\right\},$$

(D12)

$$\zeta_n^{23} = O_5\Big\{ H_1(-1+n)F_{22}(\kappa,H-h,1+n,2) + H_{21}(-1+n)F_3(\kappa,H-h,1+n,2) - H_4F_{22}(\kappa,-h,n,2) - H_{51}F_3(\kappa,-h,n,2)\Big\}$$
$$+ O_4\left\{\begin{array}{l} H_1\left[\frac{1}{2}n(1+n)^2F_1(\kappa,H-h,1+n,0) + \frac{1}{2}(1-n)F_{22}(\kappa,H-h,1+n,2)\right] + H_{22}(-1+n)F_3(\kappa,H-h,1+n,2) - H_3F_4(\kappa,H-h,n,1) \\ +H_4\left[-\frac{1}{2}n(1+n)F_1(\kappa,-h,n,0) + \frac{1}{2}F_{22}(\kappa,-h,n,2)\right] - H_{52}F_3(\kappa,-h,n,2) - H_6F_4(\kappa,-h,n,1) \end{array}\right\}, \tag{D13}$$

$$\zeta_n^{31} = O_7\left\{\begin{array}{l} I_1\left[\frac{(-1-n)F_{22}(\kappa,H-h,n,2)}{2(-1+2n)} + \frac{3F_{22}(\kappa,H-h,n,2)}{n(-1+2n)} + \frac{(-1-n)F_{22}(\kappa,H-h,1+n,1)}{-1+2n} + \frac{(-2+n)(1+2n)(H-h)F_{22}(\kappa,H-h,1+n,2)}{2n(-1+2n)}\right] \\ +\frac{1}{2n(-1+2n)}I_2\left[\left(-6+n+n^2\right)F_3(\kappa,H-h,n,2) + 2n(1+n)F_3(\kappa,H-h,1+n,1) + (2+(3-2n)n)(H-h)F_3(\kappa,H-h,1+n,2)\right] \\ +\frac{1}{2(-1+n)n(-1+2n)}I_4\left[\left(-4+n^2\right)F_{22}(\kappa,-h,-1+n,2) + 2\left(-1+n^2\right)F_{22}(\kappa,-h,n,1) + (2+(3-2n)n)(-h)F_{22}(\kappa,-h,n,2)\right] \\ -\frac{I_5\left[\left(-4+n^2\right)F_3(\kappa,-h,-1+n,2) + 2\left(-1+n^2\right)F_3(\kappa,-h,n,1) + (2+(3-2n)n)(-h)F_3(\kappa,-h,n,2)\right]}{2(-1+n)n(-1+2n)} \end{array}\right\}$$
$$+ O_6\left\{\begin{array}{l} I_1\left[\begin{array}{l}\frac{(-2+n)(1+n)^2F_1(\kappa,H-h,n,0)}{4(-1+2n)} + \frac{(2-n)(1+n)(1+2n)(H-h)F_1(\kappa,H-h,1+n,0)}{4(-1+2n)} + \frac{(-1-n)F_{21}(\kappa,H-h,1+n,1)}{-1+2n} \\ -\frac{3F_{22}(\kappa,H-h,n,2)}{2n(-1+2n)} + \frac{(1+n)F_{22}(\kappa,H-h,n,2)}{4(-1+2n)} + \frac{(2-n)(1+2n)(H-h)F_{22}(\kappa,H-h,1+n,2)}{4n(-1+2n)}\end{array}\right] \\ -\frac{1}{2n(-1+2n)}I_2\left[\left(-6+n+n^2\right)F_3(\kappa,H-h,n,2) + 2n(1+n)F_3(\kappa,H-h,1+n,1) + (2+(3-2n)n)(H-h)F_3(\kappa,H-h,1+n,2)\right] \\ +\frac{1}{2}I_3\left[\frac{\left(2+n-n^2\right)F_4(\kappa,H-h,-1+n,1)}{n(-1+2n)} + (H-h)F_4(\kappa,H-h,n,1)\right] \\ +I_4\left[\frac{(2-n)n(nF_1(\kappa,-h,-1+n,0) - (1+2n)(-h)F_1(\kappa,-h,n,0)) + 4(1+n)F_{21}(\kappa,-h,n,1)}{4n(-1+2n)} - \frac{\left(-4+n^2\right)F_{22}(\kappa,-h,-1+n,2)}{4(-1+n)n(-1+2n)} - \frac{(2+(3-2n)n)(-h)F_{22}(\kappa,-h,n,2)}{4(-1+n)n(-1+2n)}\right] \\ +\frac{I_5\left[\left(-4+n^2\right)F_3(\kappa,-h,-1+n,2) + 2\left(-1+n^2\right)F_3(\kappa,-h,n,1) + (2+(3-2n)n)(-h)F_3(\kappa,-h,n,2)\right]}{2(-1+n)n(-1+2n)} \\ +\frac{1}{2}I_6\left[\frac{\left(2+n-n^2\right)F_4(\kappa,-h,-1+n,1)}{n(-1+2n)} + (-h)F_4(\kappa,-h,n,1)\right] \end{array}\right\}, \tag{D14}$$

$$\zeta_n^{32} = O_7\Big\{ -I_1nF_{22}(\kappa,H-h,2+n,2) + I_2nF_3(\kappa,H-h,2+n,2) + I_4F_{22}(\kappa,-h,1+n,2) - I_5F_3(\kappa,-h,1+n,2)\Big\}$$
$$+ O_6\left\{\begin{array}{l} I_1\left[\frac{1}{2}n(1+n)(2+n)F_1(\kappa,H-h,2+n,0) + \frac{1}{2}nF_{22}(\kappa,H-h,2+n,2)\right] - I_2nF_3(\kappa,H-h,2+n,2) - I_3nF_4(\kappa,H-h,1+n,1) \\ +I_4\left[-\frac{1}{2}n(1+n)F_1(\kappa,-h,1+n,0) - \frac{1}{2}F_{22}(\kappa,-h,1+n,2)\right] + I_5F_3(\kappa,-h,1+n,2) - I_6nF_4(\kappa,-h,1+n,1) \end{array}\right\}, \tag{D15}$$

$$\zeta_n^{33} = O_7\Big\{ I_1(-1+n)F_{22}(\kappa,H-h,1+n,2) + I_2(1-n)F_3(\kappa,H-h,1+n,2) - I_4F_{22}(\kappa,-h,n,2) + I_5F_3(\kappa,-h,n,2)\Big\}$$
$$+ O_6\left\{\begin{array}{l} I_1\left[\frac{1}{2}n(1+n)^2F_1(\kappa,H-h,1+n,0) + \frac{1}{2}(1-n)F_{22}(\kappa,H-h,1+n,2)\right] + I_2(-1+n)F_3(\kappa,H-h,1+n,2) - I_3F_4(\kappa,H-h,n,1) \\ I_4\left[-\frac{1}{2}n(1+n)F_1(\kappa,-h,n,0) + \frac{1}{2}F_{22}(\kappa,-h,n,2)\right] - I_5F_3(\kappa,-h,n,2) - I_6F_4(\kappa,-h,n,1) \end{array}\right\}. \tag{D16}$$

Abramowitz, M. and Stegun, I. A., *Handbook of Mathematical Functions with Formulas, Graphs, and Mathematical Tables* (U.S. Government Printing Office, Wathington, D.C., 1970).

Alobaid, F., Ströhle, J., and Epple, B., "Extended CFD/DEM model for the simulation of circulating fluidized bed," Adv. Powder Technol. **24**(1), 403–415 (2013).

Amir, M., Nikora, V. I., and Stewart, M. T., "Pressure forces on sediment particles in turbulent open-channel flow: A laboratory study," J. Fluid Mech. **757**, 458–497 (2014).

Avron, J. E., Kenneth, O., and Oaknin, D. H., "Pushmepullyou: An efficient micro-swimmer," New J. Phys. **7**(1), 234 (2005).

Beetstra, R., Hoef, M. A. V. D., and Kuipers, J. A. M., "Numerical study of segregation using a new drag force correlation for polydisperse systems derived from lattice-Boltzmann simulations," Chem. Eng. Sci. **62**(1-2), 246–255 (2007a).

Beetstra, R., Hoef, V. D. M. M., and Kuipers, J. H., "Drag force of intermediate Reynolds number flow past mono- and bidisperse arrays of spheres," AICHE J. **53**(2), 489–501 (2007b).

Bernardo, B. D. L. and Moraes, F., "Simplified model for the dynamics of a helical flagellum," Am. J. Phys. **79**(7), 736–740 (2011).
Blake, J. R. and Chwang, A. T., "Fundamental singularities of viscous flow," J. Eng. Math. **8**(1), 23–29 (1974).
Brenner, H., "The Stokes resistance of a slightly deformed sphere," Chem. Eng. Sci. **19**(8), 519–539 (1964).
Cello, F., Renzo, A. D., and Maio, F. P. D., "A semi-empirical model for the drag force and fluid–particle interaction in polydisperse suspensions," Chem. Eng. Sci. **65**(10), 3128–3139 (2010).
Chan-Braun, C., García-Villalba, M., and Uhlmann, M., "Force and torque acting on particles in a transitionally rough open-channel flow," J. Fluid Mech. **684**(10), 441–474 (2011).
Chan-Braun, C., García-Villalba, M., and Uhlmann, M., "Spatial and temporal scales of force and torque acting on wall-mounted spherical particles in open channel flow," Phys. Fluids **25**(7), 075103 (2013).
Chaudhry, M. H., *Open-Channel Flow* (Springer, New York, 2008).
Daddi-Moussa-Ider, A., Lisicki, M., and Gekle, S., "Hydrodynamic mobility of a sphere moving on the centerline of an elastic tube," Phys. Fluids **29**(11), 111901 (2017).
Dandy, D. S. and Dwyer, H. A., "A sphere in shear flow at finite Reynolds number: Effect of shear on particle lift, drag, and heat transfer," J. Fluid Mech. **216**, 381–410 (1990).
Dey, S., *Fluvial Hydrodynamics: Hydrodynamic and Sediment Transport Phenomena* (Springer-Verlag, Berlin, 2014).
Di Felice, R., "The voidage function for fluid-particle interaction systems," Int. J. Multiphase Flow **20**(1), 153–159 (1994).
Drake, T. G. and Calantoni, J., "Discrete particle model for sheet flow sediment transport in the nearshore," J. Geophys. Res. Oceans **106**(C9), 19859–19868, https://doi.org/10.1029/2000jc000611 (2001).
Dwivedi, A., Melville, B. W., Shamseldin, A. Y., and Guha, T. K., "Drag force on a sediment particle from point velocity measurements: A spectral approach," Water Resour. Res. **46**(10), 79–93, https://doi.org/10.1029/2009wr008643 (2010).
Elgeti, J., Winkler, R. G., and Gompper, G., "Physics of microswimmers–single particle motion and collective behavior: A review," Rep. Prog. Phys. **78**(5), 056601 (2015).
Erdélyi, A., Magnus, V., Oberhettinger, F., and Tricomi, F., *Tables of Integral Transforms*, Fourier, Laplace, Mellin Transforms (McGraw-Hill, New York, 1954), Vol. 1.
Ergun, S., "Fluid flow through packed columns," Chem. Eng. Prog **48**(2), 89–94 (1952).
Esteghamatian, A., Hammouti, A., Lance, M., and Wachs, A., "Particle resolved simulations of liquid/solid and gas/solid fluidized beds," Phys. Fluids **29**(3), 033302 (2017).
Felderhof, B. U., "Swimming at small Reynolds number of a planar assembly of spheres in an incompressible viscous fluid with inertia," Phys. Fluids **29**(9), 091901 (2017).
Ganatos, P., "A numerical-solution technique for three-dimensional Stokes flows, with application to the motion of strongly interacting spheres in a plane," J. Fluid Mech. **84**(1), 79–111 (1978).
Ganatos, P., Pfeffer, R., and Weinbaum, S., "A strong interaction theory for the creeping motion of a sphere between plane parallel boundaries. Part 2. Parallel motion," J. Fluid Mech. **99**(4), 755–783 (1980).
Gidaspow, D., "Hydrodynamics of fluidization and heat transfer: Supercomputer modeling," Appl. Mech. Rev. **39**(1), 1–23 (1986).
Goldman, A. J., Cox, R. G., and Brenner, H., "Slow viscous motion of a sphere parallel to a plane wall—II Couette flow," Chem. Eng. Sci. **22**(4), 653–660 (1967).
Guo, Y., Wu, C. Y., and Thornton, C., "Modeling gas-particle two-phase flows with complex and moving boundaries using DEM-CFD with an immersed boundary method," AICHE J. **59**(4), 1075–1087 (2013).
Happel, J. and Brenner, H., *Low Reynolds Number Hydrodynamics* (Springer, New York, 1983).
Henry, C. and Minier, J.-P., "Progress in particle resuspension from rough surfaces by turbulent flows," Prog. Energy Combust. Sci. **45**, 1–53 (2014).
Hill, R. J., Koch, D. L., and Ladd, A. J. C., "The first effects of fluid inertia on flows in ordered and random arrays of spheres," J. Fluid Mech. **448**, 213–241 (2001).
Ikeda, S. and Mcewan, I. K., *Flow and Sediment Transport in Compound Channels: The Experiences of Japanese and UK Research* (IAHR Monograph, Madrid, 2009).
Ji, C., Munjiza, A., Avital, E., Ma, J., and Williams, J. J. R., "Direct numerical simulation of sediment entrainment in turbulent channel flow," Phys. Fluids **25**(5), 056601 (2013).
Kloss, C., Goniva, C., Hager, A., Amberger, S., and Pirker, S., "Models, algorithms and validation for opensource DEM and CF D-DEM," Prog. Comput. Fluid Dyn. Int. J. **12**(2/3), 140–152 (2012).
Lauga, E., "Bacterial hydrodynamics," Annu. Rev. Fluid Mech. **48**(1), 105–130 (2016).
Lauga, E. and Squires, T. M., "Brownian motion near a partial-slip boundary: A local probe of the no-slip condition," Phys. Fluids **17**(10), 103102 (2005).
Lee, H. and Balachandar, S., "Effects of wall roughness on drag and lift forces of a particle at finite Reynolds number," Int. J. Multiphase Flow **88**, 116–132 (2017).
Leighton, D. and Acrivos, A., "The lift on a small sphere touching a plane in the presence of a simple shear flow," Z. Angew. Math. Phys. Zamp **36**(1), 174–178 (1985).
Liu, X., Ji, C., Xu, X., Xu, D., and Williams, J. J. R., "Distribution characteristics of inertial sediment particles in the turbulent boundary layer of an open channel flow determined using Voronoï analysis," Int. J. Sediment Res. **32**(3), 401–409 (2017).
Merritt, W. S., Letcher, R. A., and Jakeman, A. J., "A review of erosion and sediment transport models," Environ. Modell. Softw. **18**(8), 761–799 (2003).
Morsi, S. A. and Alexander, A. J., "An investigation of particle trajectories in two-phase flow systems," J. Fluid Mech. **55**(2), 193–208 (1972).
Nielsen, P., *Coastal Bottom Boundary Layers and Sediment Transport* (World Scientific Pub Co, Inc., Singapore, 1992).
O'Brien, V., "Form factors for deformed spheroids in Stokes flow," AICHE J. **14**(6), 870–875 (1968).
O'Neill, M. E., "A sphere in contact with a plane wall in a slow linear shear flow," Chem. Eng. Sci. **23**(11), 1293–1298 (1968).
Purcell, E. M., "Life at low Reynolds number," Am. J. Phys. **45**(1), 3–11 (1977).
Renzo, A. D., Cello, F., and Maio, F. P. D., "Simulation of the layer inversion phenomenon in binary liquid–fluidized beds by DEM–CFD with a drag law for polydisperse systems," Chem. Eng. Sci. **66**(13), 2945–2958 (2011).
Sun, R. and Xiao, H., "Sediment micromechanics in sheet flows induced by asymmetric waves: A CFD–DEM study," Comput. Geosci. **96**, 35–46 (2016).
Takemura, F. and Magnaudet, J., "The transverse force on clean and contaminated bubbles rising near a vertical wall at moderate Reynolds number," J. Fluid Mech. **495**, 235–253 (2003).
Turkyilmazoglu, M., "Unsteady flow over a decelerating rotating sphere," Phys. Fluids **30**(3), 033601 (2018).
Villar, R. E., Martinez, J. M., Guyot, J. L., Fraizy, P., Armijos, E., Crave, A., Bazán, H., Vauchel, P., and Lavado, W., "The integration of field measurements and satellite observations to determine river solid loads in poorly monitored basins," J. Hydrol. **444-445**(6), 221–228 (2012).
Vladimirov, V. A., "Dumbbell micro-robot driven by flow oscillations," J. Fluid Mech. **717**(1), R8 (2013).
Wakiya, S., "Effect of a plane wall on the impulsive motion of a sphere in a viscous fluid," Tokyo Sugaku Kaisya Zasshi **19**(8), 1401–1408 (1964).
Weller, H. G., Tabor, G., Jasak, H., and Fureby, C., "A tensorial approach to computational continuum mechanics using object-oriented techniques," Comput. Phys. **12**(6), 620–631 (1998).
Wen, C. Y. and Yu, Y. H., "Mechanics of fluidization," Chem. Eng. Prog. Symp. Ser **62**, 100–111 (1966).
Xu, B. H., Yu, A. B., Chew, S. J., and Zulli, P., "Numerical simulation of the gas–solid flow in a bed with lateral gas blasting," Powder Technol. **109**(1-3), 13–26 (2000).
Yang, S. M. and Leal, L. G., "Particle motion in Stokes flow near a plane fluid-fluid interface. Part 2. Linear shear and axisymmetric straining flows," J. Fluid Mech. **149**(149), 275–304 (1984).
Zeng, L., Balachandar, S., and Fischer, P., "Wall-induced forces on a rigid sphere at finite Reynolds number," J. Fluid Mech. **536**, 1–25 (2005).
Zeng, L., Najjar, F., Balachandar, S., and Fischer, P., "Forces on a finite-sized particle located close to a wall in a linear shear flow," Phys. Fluids **21**(3), 033302 (2009).